NASA-CR-193626

(NASA-CR-193626) PHYSICS OF FOREBODY FLOW CONTROL (MCAT Inst.) 45 p

N94-11195

Unclas

G3/02 0179685

MCAT Institute
Progress Report
93-12

Physics of Forebody Flow Control

Gabriel I. Font

August 1993

NCC2-729

MCAT Institute
3933 Blue Gum Drive
San Jose, CA 95127

PHYSICS OF FOREBODY FLOW CONTROL

by

Gabriel I. Font

Introduction

Performance in the high angle of attack regime is required by many different types of aircraft. Military aircraft, such as fighters, utilize flight in this regime to improve maneuverability. Civilian aircraft, such as supersonic or hypersonic transports, will also need to operate in this regime during take off and landing, due to their small highly swept wings. Flight at high angles of attack is problematic due to the vortices being created on the nose of the aircraft. These vortices tend to become asymmetric and produce side forces. At the same time, the rudders are less effective because they are becoming immersed in the flow separating from the wings and fuselage. Consequently, the side force produced by the vortices on the nose tend to destabilize the aircraft. This situation may be corrected through the use of a forebody flow control system such as tangential slot blowing. In this concept, a jet is blown from the nose in an effort to alter the flow field around the nose and diminish the destabilizing side force. Alternately, the jet may be used to create a side force which could be used to augment the rudders. This would allow the size of the rudders to be decreased which would, in turn, diminish the cruise drag. Therefore, the use of a tangential slot blowing system has the potential for improving both the maneuver performance and the cruise performance of an aircraft.

Present Work

The present study was conducted to explore the physics of forebody flow control. The study consisted of two major thrusts:

- Exploration of forebody flow control with tangential slot blowing.
- Investigation of flow field response to a general perturbation.

Forebody Flow Control

The first thrust explored issues dealing with tangential slot blowing. A tangent-ogive cylinder configuration was utilized for which experimental measurements were available. The compressible Thin-Layer, Reynolds-Averaged, Navier-Stokes equations were solved numerically on this configuration. A theory detailing the force production mechanisms was developed. This theory also explained their relative importance and contribution to the total force production. Also explored in this thrust were the effects on force production of: 1) angle of attack, 2) slot location and 3) jet blowing strength. The details of the study were published and are included in Appendix A. The results of this study will be useful in the optimization and installation of tangential slot blowing system.

During the course of the study, a question was raised about the effects of the numerical treatment of the aft end of the body. Many studies had been conducted, including the present one, where the aft end of the body was not included in the computation.[1-5] Such treatment had the effect of removing the influence of the tail geometry and wake from the computations. A companion study was launched to identify and quantify these effects. Computations in which the aft end of the body was included were carried out. The configuration (with the exception of the aft end of the body) and flow conditions were identical to the ones in the first part of the present study. Comparisons were made between the two sets of computations. It was concluded that the omission of the aft end of the geometry did not change the fundamental physics of the force production although it affected the force levels. The details of this companion study were also published and are included in Appendix B.

Flow Response to a Disturbance

The second thrust consisted of a fundamental examination of the behavioral characteristics of the flow field. If the characteristics of flow field response to general perturbations were known, a flow control system could be designed to take advantage of them in the most efficient manner. The guess work inherent in the design of such a system would be removed and the design period would be shortened.

Adjoint eigensolutions of the governing equations are capable of characterizing the perturbation receptivity properties of the steady flow field. This method has been shown to be especially applicable to flow fields containing large separated regions. A single

solution of the adjoint set of equations would provide information about the quasi-linear response of the flow field to a general perturbation. Consequently, a large amount of initial solutions would not be required to determine the behavior of a flow field away from an initial steady state. This would greatly diminish the computational effort needed to explore the response of the flow field to a new or different flow control concept, such as blowing, suction, or wall perturbation. This general approach has been demonstrated for analytically describable configurations in two dimensions.[6] The present work prepares the way for the treatment of general configurations in two dimensions with the eventual goal of applying it to three-dimensional general configurations.

The mathematical theory was developed with the assistance of D. C. Hill. This resulted in a set of equations which was adjoint to the Navier-Stokes equations while at the same time was not inherently unstable if marched in time. The theory for the numerical treatment of this set of equations was then developed. Issues involving discretization, coordinate transformation, flux linearization, factorization, and implicit formulation of the governing set of equations were resolved. Initial stability analysis of the time marching scheme was also carried out. At the conclusion of this study, problems with numerical stability had not been solved. Details of the mathematical theory and numerical formulation can be found in Appendix C.

References

1. Tavella, D. A., Schiff, L. B. and Cummings, R.,"Pneumatic Vortical Flow Control at High Angles of Attack," AIAA Paper No. 90-0098, 28th Aerospace Sciences Meeting, January 1990

2. Gee, K., Tavella, D. A. and Schiff, L. B., "Computational Optimization of a Pneumatic Fuselage Forebody Flow Control Concept," AIAA Paper No. 91-3249, 9th Applied Aerodynamics Conference, September 1991.

3. Degani, D., "Numerical Investigation of the Origin of Vortex Asymmetry," AIAA Paper No. 90-0593, AIAA 28th Aerospace Sciences Meeting, January 1990.

4. Font, G. I., and Tavella, D. A., "High Alpha Aerodynamic Control by Tangential Fuselage Blowing," *AIAA Journal*, Vol. 30, No. 5, May 1992, pp. 1321-1330.

5. Font, G. I., Celik, Z. Z., and Roberts, L. "A Numerical and Experimental Study of Tangential Jet Blowing Applied to Bodies at High Angles of Attack," AIAA Paper No. 91-3253, 9th Applied Aerodynamics Conference, September 1991.

6. Hill, D. C., "A Theoretical Approach for Analyzing the Restabilization of Wakes," AIAA Paper No. 92-0067, 30th Aerospace Sciences Meeting, January 1992.

APPENDIX A

AIAA-92-4648

Force Production Mechanisms of a Tangential Jet on Bodies at High Algha

G. I. Font
Stanford University
Stanford, California

Atmospheric Flight Mechanics Conference
August 10-12, 1992/Hilton Head, SC

Force Production Mechanisms of a Tangential Jet on Bodies at High Alpha

G. I. Font*

Department of Aeronautics and Astronautics

Stanford University, Stanford CA 94305

Abstract

This work explores the mechanisms by which tangential slot blowing creates forces on a body at a high angle of attack. The study is conducted numerically by solving the three-dimensional, compressible-flow Navier-Stokes equations. A tangent-ogive cylinder configuration is used with the blowing slot located both on the nose and on the cylindrical part of the body. The angle of attack used is 30 deg., the Mach no. is 0.2 and the Reynolds no., based on diameter, is 52000. Several conclusions were made concerning the physical mechanisms by which the jet interacts with the ambient flow field to produce a side force: (1) A centrifugal force component is created at the wall due to the momentum of the jet being forced to follow the curvature of the surface. (2) A large amount of vorticity is added to the flow field by the jet. In the region of the slot, the vorticity has the effect of inducing circulation around the body. Downstream of the slot, the vorticity alters the strength of the nose vortices. (3) The position of the nose vortices can be altered do to the jet changing the location of separation. And (4), the jet has the ability to excite unstable behavior producing a global change in the character of the flow.

Nomenclature

c_y	sectional side force coefficient: $\mathrm{d}(C_y)/\mathrm{d}x$
C_y	side force coefficient: Force/$q_\infty S_{ref}$
C_μ	blowing momentum coefficient
H	helicity density
Γ	circulation
M_∞	Mach number
Re	Reynolds number
S_j	slot area
S_{ref}	reference area
U_j	jet velocity
$\mathbf{V}$	flow velocity vector
$\mathbf{w}$	vorticity vector
r	normal distance from surface
α	angle of attack, degrees
ρ	density

Subscripts

D	diameter of the model
j	jet
∞	freestream reference conditions

* Research Scientist. Member AIAA.

Introduction

The continuing need to increase the maneuverability of aircraft requires that they be flown at ever increasing angles of attack. At high angles of attack, however, the control surfaces, namely the rudders and elevators, become immersed in separated flow. This renders them ineffective in controlling the aircraft. Complicating the situation further, are the vortices emanating from the nose which, at high angles of attack, tend to become asymmetric, creating a side force which makes the aircraft prone to departure from controlled flight.

This problem can be alleviated by either providing supplementary control mechanisms or decreasing the required control forces. One system which capable of doing both is tangential slot blowing. The concept of tangential blowing involves injecting a thin jet tangential to the surface from a slot situated longitudinally along the body, as shown in Figure 1. The jet initially will follow the curvature of the surface and later will separate. In the process, the asymmetry in the nose may be diminished or enlarged in order to reduce an unwanted side force or provide one which can be used to control the aircraft.

Previous Work

Many studies have been conducted in an effort to explore the capabilities of a pneumatic system for the production of a side force. A few examples of these studies are Ref. 1-11. In the course of these studies, several mechanisms have been proposed to explain how a tangential jet produces a side force on a body at a high angle of attack. Ref. 1 studied the problem of a tangential jet in a two dimensional fashion and concluded that the effects of the jet could be characterized as a creation of circulation around the cylinder. References 2-4, while studying a discrete jet located on the nose of a body, proposed that the flow could amplify perturbations, such as that provided by a jet. Ref. 5 determined that the symmetric flow field was convectively unstable and that a perturbation at the nose could cause a shift to the asymmetric state. Ref. 6 also studied a jet located on the nose of the body, but instead of a discrete jet, a jet blowing from a slot was used. The authors suggested that the main function of the jet was to alter the separation pattern and change the position of the vortices on the lee side of the body. Ref. 7 - 9 studied a slot-jet located aft of the nose. The authors concluded that a major mechanism for the interaction of the jet with the ambient flow field was the vorticity released by the jet.

Present Work

The objective of the present work is to study the physical mechanisms which result in force production by

tangential jet blowing. An understanding of these mechanisms will result in an system better optimized to the mission requirements and installation restrictions. This study was conducted by numerically solving the compressible, Reynolds-averaged, thin-layer Navier-Stokes equations. The code used is F3D. It is fully described in Ref. 12-14 and will not be detailed further here. Comparison of the computation with experiments for the current configuration, and flow solver were carried out in Ref. 10. The angle of attack used in the present computations is 30 deg., the Mach no. is 0.2 and the Reynolds no. is 52000. These conditions were chosen to facilitate comparison with previous studies.[8,10,11] The grid contains 52, 100, and 60 points in the axial, circumferential, and normal directions, respectively. The outer boundaries are 20 body diameters from the surface. The exit plane is located at the end of the body. Solution of the flow field is accomplished in a zonal manner. Communication between the zones is carried out through a one cell overlap. The jet is implemented with the actuator plane method first detailed in Ref. 7. In this method, a zonal boundary is made to coincide with the location of the slot. The jet flow variables are then entered as a boundary condition on the computational cells which match the slot exit. The turbulence in the jet is handled with the eddy viscosity model due to Roberts[15], while the eddy viscosity in the boundary layers is calculated with the Baldwin-Lomax model[16] with Degani-Schiff modifications [17].

The body chosen for the investigation is the tangent-ogive cylinder. The simple configuration facilitates the isolation of the physical effects from those due to the geometry. It also lowers the numerical cost, allowing for a more detailed investigation of the phenomenon. The configuration is illustrated in Figure 2. Two slot locations are employed in the investigation: one at the nose and the other at the cylinder-ogive junction. Both slots are located 90 deg. circumferentially from the windward plane of symmetry and are of constant thickness. The cases with the slot at the cylinder-ogive junction were reported previously[8], but will be used in this work for comparison with the cases where the slot is located at the nose. The jet momentum coefficient is defined as

$$C_\mu = \frac{\rho_j u_j^2 S_j}{\frac{1}{2}\rho_\infty V_\infty^2 S_{ref}} \qquad (1)$$

where ρ_j, u_j, and S_j refer to the density, mean velocity, and the slot area of the jet, respectively. The reference area, S_{ref}, is the body diameter multiplied by the body slot length. The same reference area will be used for both the body-slot and the nose-slot cases to allow comparison between the two.

Results

Ref. 8 identified one mechanism for force production as the centrifugal force component. It is fully discussed there and is only mentioned here for completeness. Briefly, a discontinuity, with respect to the circumferential angle around the body, was found in the surface pressure contours in the region of the slot and only where the jet was present. An estimate was made of the centrifugal force by carrying out a force balance on a differential element of the fluid in the jet as it was forced to negotiate the curvature of the body. The magnitude of this estimate was found to agree closely with the magnitude of the discontinuity in the pressure distribution. Consequently, it was concluded that the source of the discontinuity was the centrifugal force component created by the presence of the jet. As the angle of attack increased, the contribution of the centrifugal component to the local force diminished due to the early separation of the jet. The cross-sectional pressure distributions, indicated that at $\alpha = 10°$, the centrifugal force component was more than 50% of the local side force, while at $\alpha = 45°$, it was less than 30%. This mechanism for force production is only important for the cases where the surface curvature is not excessive and in flow conditions where the jet remains attached a significant distance. At very high angles of attack, for example, the jet does not remain attached very long and consequently the centrifugal component of the side force is diminished. Similarly, in the cases where the slot was located in the nose, the extreme curvature caused early jet separation. Consequently, the contribution made by the centrifugal force toward the total force generated by the jet for these cases is also negligible.

Creation of Circulation

Through inspection of the surface streamlines, insight may be gained into another mechanism by which the jet interacts with the ambient flow to produce a side force. Figure 3 shows the surface streamlines for the no-blowing and the blowing cases. The cases pertain to both the body-slot and the nose-slot geometries. In both geometries, a clear effect of blowing is to shift the location of the primary separation line on the slot-side of the body. This effect is most pronounced in the vicinity of the slot but is also present downstream of the slot. (The location of the separation lines on the opposite side of the body are also shifted but the discussion will only refer to the slot-side separations.) Moving the separation lines can produce a side force by two methods. First, the as the boundary layers are forced to remain attached longer, the pressure along the body is reduced further. This effect is significant in the body-slot cases where the change in separation line location is most pronounced. In the nose-slot case, however, changing the position of separation is not important with respect to decreasing the pressure along the surface in the slot region since the jet remains attached for such a small distance. The second method of producing a side force entails the nose vortices. These vortices are fed from the sheets of fluid that leave the surface at the separation lines. By changing the position of the separation lines, the trajectory of these sheets and the position of the vortices also change. This mechanism for producing a side force will be addressed in the section dealing with the interaction of the jet-supplied vorticity with the ambient flow.

Changing the position of the separation lines is equivalent to inducing circulation about the body. On a lifting wing, the sharp trailing edge fixes the separation point and determines the amount of circulation induced about the airfoil. In the case under study, it is the jet which fixes the separation point and, in turn, determines the amount of "circulation" induced about the body. The circulation induced around the body and its distribution in the flow field can be accurately quantified by directly computing the circulation. Circulation is defined as,

$$\Gamma \equiv -\oint_C \mathbf{V} \cdot d\mathbf{s} \qquad (2)$$

This integral will be evaluated on concentric paths at different perpendicular distances, r, from the surface as shown in Figure 4a. This set of concentric integrals will be carried out at five different stations along the body. The first station is immediately before the slot. The second is in the middle of the slot, while the rest are downstream of the slot (Figure 4b). Figure 4c shows the locations of the integration for the nose-slot case.

Figure 5 shows the normalized circulation vs distance from the surface calculated for a case where the slot is located at the cylinder-ogive junction and the angle of attack is 30°. These cases are fully detailed in Ref. 11. Figure 5a shows the case with no blowing. As expected, because of the symmetric flow, no net circulation is found at any station along the body or any distance from the body. Figure 5b shows the circulation for the case where $C_\mu = 0.1$. Immediately before the slot, x/L=0.26, (the slot is located between x/L=0.28 and 0.46) the circulation is negligible at every distance from the body. Half way along the slot, x/L=0.35, a circulation peak of $\Gamma/a_\infty l_{ref} = 0.3$ is found at a distance on the order of 10^{-2} diameters from the surface. This coincides with the location of the maximum velocity of the jet. Downstream of the slot, at x/L=0.55, the circulation peak is diminished slightly in magnitude and is found at a greater distance from the surface (10^{-1} diameters) than at the previous station. Aft of this fuselage station, the circulation peaks continue to move away from the surface. By the end of the body, the peak is located at a distance on the order 0.5 diameters from the surface. Figures 5c and 5d show the circulation distribution for the C_μ = 0.2 and 0.4 cases, respectively. The same characteristics as in the previous case are exhibited: A large circulation peak is created in the region of the slot very close to the surface. This peak diminishes and moves away from the surface as it travels downstream. At a large distance from the surface, r/D, the circulation is always zero indicating that the net vorticity created by the jet is zero, as expected. This figure shows that any potential flow model assuming a bound vortex would only be accurate in the region of the slot. Downstream of the slot the model would have to be modified to allow the shedding of the bound vortex.

The fact that the circulation starts out as bound and then moves away from the surface suggests a conceptual model which may be used to explain this component of the interaction of the jet with the ambient flow field. Figure 6a shows a lifting wing with a nearly constant lift distribution. The bound vortex does not end in the wing but continues downstream through the wing tip vortices. Figure 6b shows a body with a nearly constant side force distribution. Its bound vortex also does not end in the body but continues downstream through trailing vortices. The trailing vortex farther from the surface is created in the shear layer between the jet maximum velocity and the ambient flow, as suggested by the inset in Figure 6b, while the vortex in the boundary layers and the vortex that trails closer to the surface is created in the shear layer between the jet maximum velocity and the surface. Figure 7 illustrates how such a model can explain the circulation behavior noted in Figure 5. At a station along the slot, x_1 in Figure 7a, the circulation line integral would first encounter the positive bound vortex which would raise the circulation content, shown schematically in Figure 7b. Then, as the equal negative vortex was encountered farther away from the surface, the circulation content would return to zero. At a station farther downstream, x_2, the integral would have to be at a farther distance from the surface, r/D, before it began to sum over the positive vortex. As in the previous case, as the integration proceeded over the negative trailing vortex, the total circulation would, again, return to zero. The jet appears to be creating a bound vortex in the region of the slot. This vortex can not end the slot region and, therefore, continues downstream while moving away from the surface.

Jet Vorticity Interaction with Ambient Flow

The previous section established that the jet was creating vorticity in the flow field. An estimate for the quantity of vorticity created can be obtained by integrating the vorticity through out the flow field. However, since equal amounts of both positive and negative vorticity are produced, a simple integral would always show zero net vorticity. Since by Stokes' theorem the line integral in eqn. 2 may be recast as,

$$\Gamma \equiv - \int \int_A \mathbf{w} \cdot d\mathbf{A} \tag{3}$$

an estimate for the net vorticity content at a particular x station may be obtained by noting the value of this integral far away from the body. As shown by Figure 5b, the net vorticity, at a large r/D, is zero at every x station. If instead, the absolute value of the vorticity is integrated, an estimate for the total vorticity in the flow field is obtained. This integral has the form,

$$G \equiv - \int \int_A | \mathbf{w_x} | \, d\mathbf{A} \tag{4}$$

Figure 8 shows the value for G at each longitudinal station along the body for the no- blowing case and the case where $C_\mu = 0.2$. In the region of the slot, the jet is shown to nearly double the vorticity content in the flow field. However, most of this vorticity is canceled near the end of the slot. The remaining, or residual, vorticity is transported downstream as shown by the increased amount of vorticity in the aftbody.

The helicity density[18] contours for the blowing cases provide a clue as to the nature of the interaction of the residual vorticity with the flow field in the aft body. Figure 9 shows the cases where the slot is located on the cylinder-ogive junction and $\alpha = 10°$. At this angle of attack, the vorticity due to the no-blowing flow field is minimal (as shown in Figure 9a) and the effects of the jet are more readily isolated. The jet, being composed of two shear layers, dumps both positive and negative vorticity into the flow field. These vortices or vortex clouds then interact with the ambient flow field. Figure 9b shows that after the positive vorticity, denoted in black, is released, it remains close to the surface, while the negative vorticity, denoted in grey, moves away from the surface. This suggests that the location at which the vorticity is released is important to the extent or nature of its interaction with the surrounding flow field. The positive vorticity is released in the shear layer between the jet maximum velocity and the surface, where the velocity components normal to the surface are

small. In the aft body, it consequently moves away from the surface at a slow rate. The negative vorticity, however, is released into the external flow where the velocity normal to the surface is higher. It is entrained by the external flow and carried away from the surface at a much faster rate.

The interaction of the jet-released vorticity with a flow field where stronger nose vortices are present can be observed in the cases computed at a higher angle of attack. Figures 10a-10d show the helicity density contours for the cases at $\alpha = 30°$. These are the same cases examined in the section dealing with circulation. At the lowest blowing strength, $C_\mu = 0.1$ in Figure 10b, the vortex on the slot side of the body is made stronger. This is indicated by the fact that the slot- side helicity structures, near the end of the body, contain a larger number of contours than their counterparts in the no-blowing case. (Because the outer contours in this figure all have the same value and the same increment between contours, a larger number of contours indicates a stronger vorticity value in the contour at the center of the vortex.) The positive vorticity furnished by the jet is apparently combining with the slot-side vortex increasing its strength, while the negative vorticity, having been released above or farther away from the body than the vortex sheet that feeds the vortex on the slot side, is carried away and is not entrained. The interaction, therefore, may be thought of as "linear". The behavior is not truly linear in the mathematical sense but this term is used to indicate that the behavior resembles a superposition of vorticity. Also, it must be recognized that the effect of the jet is not limited to strengthening the slot-side vortex. Simultaneously, the vortex on the opposite side is weakened. The positions of the vortices with respect to the surface are also altered. These effects, however, were fully described in Ref. 8 and 11 and for the sake of brevity the interaction of the jet with the flow field will be "catalogued" by its effect on the slot-side vortex. In the spirit of the discussion, however, the entire effect of the presence of the jet is being considered. At the larger blowing strengths, $C_\mu = 0.2$ and 0.4, the slot-side vortex downstream of the slot is weaker than its counterpart in the no-blowing case. This indicates a fundamental change in the interaction of the jet with the ambient flow field. The idea of simple superposition of vorticity no longer holds and a non-linear behavior is exhibited.

The sectional side force distribution in Figure 11 shows that where the linear behavior was observed, the slot side vortex was made stronger and the side force was nearly constant in the aftbody ($C_\mu = 0.1$). Conversely, where the non-linear behavior was observed, the slot side vortex was not made stronger and the side force decreased in the aftbody ($C_\mu = 0.2$ and 0.4). This establishes a relationship between the vortex strength behavior and the side force characteristics. The reason why the change in behavior takes place, however, still requires some clarification. This change in behavior was noted for the cases where $C_\mu = 0.2$ and 0.4. The circulation distributions for these cases are shown in Figures 5c and 5d. Comparison with the case where $C_\mu = 0.1$ reveals that the only difference is a negative circulation peak, in the aftbody near the surface, displayed by the cases where the change in behavior was noted. For example: the negative peak in the x/L = 0.90 curve at $r/D = 10^{-1}$ in Figure 5c. The appearance of a negative circulation peak signals the start of the non-linear behavior.

The bound vortex model, for the jet interaction with the ambient flow, stipulates that in the region of the jet, more positive vorticity will be produced at the surface than negative vorticity. (The total sum of the vorticity being produced is still zero because the outer shear layer of the jet is producing negative vorticity.) This net positive production at the surface is manifested in the circulation distribution (Figure 5) as a positive slope near the wall, for the curves in the slot region. As the vortex leaves the surface, however, the net sum of vorticity produced at the wall should return to zero as in the no-blowing case. This is indeed what happens as shown by the zero slope, near the wall, of the circulation distribution curves pertaining to the aftbody (x/L = 0.9 in Figure 5b). Therefore, the simple model of a bound vortex that leaves the surface does not provide a mechanism for the aftbody to be producing a net sum of negative vorticity at the surface of the body.

In an effort to understand the reason behind the negative circulation peak it is necessary to examine the behavior of the nose vortices in the presence of blowing. Figure 12 shows the off-body particle traces for the $\alpha = 30°$ cases. The slot, in this figure, is denoted with two parallel lines along the body. The vortex on the slot side, is shown with solid particle traces, while the vortex on the opposite side is shown with dashed particle traces. In the no-blowing case, the nose vortices are symmetric, as expected. At the lowest blowing strength, $C_\mu = 0.1$, the vortex on the slot side of the body remains close to the surface while the vortex on the opposite side begins to lift off. Because the slot-side vortex remains close to the surface, the positive vorticity furnished by the jet is able to be entrained in the slot-side vortex. Consequently, the interaction of the jet with the flow field appears additive or "linear" in nature. At $C_\mu = 0.2$, the slot-side vortex lifts off the surface at the start of the slot region, while the vortex on the opposite side lifts off at a position forward of its counterpart at the lower blowing strength. The lifting of the slot-side vortex is the reason for the change in behavior. The jet furnished vorticity can not simply combine with the nose vortex because it has left the vicinity of the surface. The helicity figures show a weaker vortex on the slot-side, for the non-linear cases, because this vortex no longer contains the vorticity coming from upstream. The vortex in the aftbody in the non-linear cases is a new vortex which has originated in the slot region, perhaps with the separation of the jet. When the slot-side vortex leaves the surface, the body begins to experience alternate shedding in space. The shedding is quasi-steady and only dependent upon position on the body. The alternate shedding of vortices is the reason behind the negative vorticity peaks that are observed in all of the cases where the side force decreases in the aftbody. If the body was sufficiently long, the surface would begin to again shed a net positive vorticity. It is possible to see this reversal in a flow field computed about an extended body. Figure 13a shows a body that is 2.42 times the length of the original body. The flow conditions are identical to those of the $\alpha = 30°$ case with $C_\mu = 0.4$. Figure 13b shows the circulation distribution for the aftbody of this case. At x/L = 0.9, a negative circulation peak is located near the surface as is observed in the short bodies. However, near the aftbody, x/L=2.32, the circulation near the surface is again positive. Therefore, the net sum of vorticity is alternating between positive and negative. Figure 13c shows the side force distribution for the

extended body case. The sectional side force alternates between positive and negative in the aftbody.

Convective Instability

The cases which employed a slot located on the nose provide information concerning another interaction mechanism of the jet. Figure 14 compares the total side force produced by the nose-slot cases with that produced by the body-slot cases. For very low jet blowing strengths, the nose slot appears to be more effecient than the slot located on the body of the model. The case with a $C_\mu = 0.005$ creates a $C_y \approx 0.80$. This side force is 160 times greater than the momentum of the jet. The reason for this apparent efficiency will be explored in this section.

Figure 15 shows the helicity density contours for the nose-slot cases. The flow features of the case where C_μ = 0.005 are not significantly different from the features of the case where the blowing strength is 40 times greater (C_μ = 0.2). The mere presence of the jet appears to be enough to cause a shift in the flow field from a symmetric configuration to an asymmetric one. Ref. 19 established that the symmetric flow field around a body at a high angle of attack was convectively unstable and that a perturbation at the nose could trigger a global change in the character of the flow. The jet in the nose-slot cases is providing the perturbation, the pneumatic bump that shifts the local flow near the nose and, in turn, changes the flow field downstream.

The theory that the jet is exciting a convective instability is supported by the circulation distribution, the side force distributions, and experiments. Figure 16 shows the circulation distribution for the nose-slot case with C_μ = 0.005. The jet produces a circulation spike along the slot, x/L = 0.12, which diminishes immediately aft of the slot, x/L = 0.32. Downstream of this station, however, the amount of circulation progressively increases. The response of the flow field to the presence of the jet grows downstream of the slot. This is characteristic of an unstable response to a perturbation. Figure 17 shows the side force distribution for the nose-slot cases. In each case, the side force drops to near zero immediately after the slot. Downstream, however, the side force begins to increase and continues to increase over much of the aftbody. Figure 14 shows the total side force vs the blowing strength for the experiments[10]. With no blowing present, the experimental body has a side force of the same order of magnitude as the side force produced by the nose-slot case with C_μ = 0.005. This side force is being caused by the geometric perturbations that exist on the surface of the body. Thus, the characteristics of the flow field due to the presence of the jet are similar to those of a flow field due to a response to a perturbation.

Figure 18 shows the numerical flow field response to a true geometric perturbation in terms of the circulation distribution. The converged flow field was provided by Ref. 19. The angle of attack, Reynolds number, and Mach number are 30°, 4(10^6), and 0.2, respectively. Figure 18 shows the circulation distribution for the geometrically perturbed body. It is clear that a perturbation can cause the circulation peaks observed in the nose-slot cases.

Summary

The examined interactions of the jet with the ambient flow can now be summarized. The jet, with its two shear layers, produces two vortices, or more exactly, vortex clouds, of equal but opposite strength. The vorticity produced in the shear layer farther away from the surface is carried away from the body and does not appear to play a large role in the production of side force. The vorticity produced in the shear layer near the surface remains in the boundary layer in the slot region and then begins to move away from the surface aft of the slot. As it moves away, it is entrained in the slot-side nose vortex increasing its strength and maintaining the side force along the aftbody. If the jet is of sufficient strength, the slot-side nose vortex leaves the surface near the beginning of the slot. The jet-furnished vorticity is consequently not entrained in this vortex. The body begins to shed vortices alternately in space and the side force diminishes in the aftbody. If the body is sufficiently long, the side force may become negative (Figure 11, C_μ = 0.4) or alternate in the aftbody (Figure 13c). This is the reason why Ref. 8 noted that at high blowing strengths or high angles of attack, the total side force could decrease with increasing C_μ. This is depicted in Figure 19 which is reprinted from Ref. 8. At α = 45° and C_μ = 0.4 the side force is lower than at C_μ = 0.2 for the same angle of attack. Finally, if the slot is located very close to the nose, the jet can produce a side force simply by perturbing the symmetric flow field into an asymmetric state. The relative importance of this force production mechanism is dependant upon the location of the slot.

Conclusions

A study of the interactions of a tangential jet with the flow field around a tangent-ogive cylinder at an angle of attack was conducted. The following conclusions were made about the interaction of the jet with the external flow and the force production mechanisms:

o Part of the jet induced side force came from the centrifugal force developed when the momentum contained in the jet was forced to follow the curvature of the body. This component was only important in the vicinity of the slot where it produced as much as 60% of the local side force. Its importance diminished, due to early separation of the jet, as the angle of attack increased or as the slot was moved toward the nose.

o The jet induced circulation about the body. The circulation was initially located in the boundary layers, but downstream of the slot, it moved away from the surface.

o The jet created a large amount of vorticity in the flow field. The majority of the jet-furnished vorticity was canceled immediately after the end of the slot. The remaining vorticity combined with the nose vortices to alter their strength.

o Part of the side force produced by the jet was due to displacing the nose vortices. If the jet blowing strength was sufficiently large, the body began to shed vortices alternately in space.

o When the slot was located near the nose, the jet was able to produce a side force by perturbing the symmetric flow field into an asymmetric state.

Acknowledgments

Many thanks are owed to L. Schiff for the support he has given to this research. This work was sponsored by NASA-Ames Research Center under NASA Contract NCC 2-55.

References

[1] Roberts, L., "The Generation of Sideforce on a Cylinder by Tangential Blowing," JIAA-TR- 102, April 1991.

[2] Moore, W. A., Skow, A. M. and Lorinez, D. J., "Enhanced Departure/Spin Recovery of Fighter Aircraft Through Control of the Forebody Vortex Orientation," AIAA Paper No. 80-0173, AIAA 18th Aerospace Sciences Meeting, January 1980.

[3] Peake, D. J., Owen, F. K., and Johnson, D. H., "Control of Forebody Vortex Orientation to Alleviate Side Forces," AIAA Paper No. 80-0183, AIAA 18th Aerospace Sciences Meeting, January 1980.

[4] Malcolm, G. N., Ng, T. T. and Murri, D. G., "Development of Non- conventional Control Methods for High Angle of Attack Flight Using Vortex Manipulation," AIAA Paper No. 89-2192, 27th Aerospace Sciences Meeting, January 1989.

[5] Degani, D., "Numerical Investigation of the Origin of Vortex Asymmetry," AIAA Paper No. 90-0593, AIAA 28th Aerospace Sciences Meeting, January 1990.

[6] Ng, T. T., and Malcolm, G. N., "Aerodynamic Control Using Forebody Blowing and Suction," AIAA Paper No. 91-0619, 29th Aerospace Sciences Meeting, January 1991.

[7] Tavella, D. A., Schiff, L. B. and Cummings, R., "Pneumatic Vortical Flow Control at High Angles of Attack," AIAA Paper No. 90-90098, 28th Aerospace Sciences Meeting, January 1990

[8] G. I. Font and D. A. Tavella, "High Alpha Aerodynamic Control by Tangential Fuselage Blowing," *AIAA Journal* **30, No. 5** (1992), 1321-1330.

[9] Gee, K., Tavella, D. A. and Schiff, L. B., "Computational Optimization of a Pneumatic Fuselage Forebody Flow Control Concept," AIAA Paper No. 91-3249, 9th Applied Aerodynamics Conference, 1991.

[10] Celik, Z. Z. and Roberts, L., "Experimental Results of the Control of Lateral Forces on a Slender Body," JIAA-TR-100, January 1991.

[11] G. I. Font, Z. Z. Celik and L. Roberts, "Numerical and Experimental Study of Tangential Jet Blowing Applied to Bodies at High Alpha," AIAA Paper No. 91-3253, 9th Applied Aerodynamics Conference, September 1991.

[12] Steger, J. L., Ying, S. X., and Schiff, L. B., "A Partially Flux-Split Algorithm for Numerical Simulation of Unsteady Viscous Flows," *Proceedings of a Workshop on Computational Fluid Dynamics*, University of California, Davis, 1986.

[13] Ying, S. X., "Three-Dimensional Implicit Approximately Factored Schemes for Equations in Gasdynamics," Ph.D. Thesis, Stanford University, 1986 (also SUDAAR 557, June 1986).

[14] Ying, S. X., Baganoff, D., Steger, J. L., and Schiff, L. B., " Numerical Simulation of Unsteady, Viscous, High-Angle- of-Attack Flows Using a Partially Flux-Split Algorithm," AIAA Paper 86-2179-CP, AIAA Atmospheric Flight Mechanics Conference, Aug. 1986.

[15] Roberts, L., "A Theory for turbulent Curved Wall Jets," AIAA Paper No. 87-0004, 1987.

[16] Baldwin, B. S. and Lomax, H., "Thin Layer Approximation and Algebraic Model for Separated Turbulent Flows," AIAA Paper 78-257, AIAA 16th Aerospace Sciences Meeting, Jan. 1978.

[17] Degani, D. and Schiff, L. B., "Computation of Turbulent Supersonic Flows Around Pointed Bodies Having Crossflow Separation," *J. Comp. Phys.* **66** (1986), 173-196.

[18] Levy, Y., Degani, D. and Seginer, A., "Graphical Visualization of Vortical Flows by Means of Helicity," *AIAA J.*, Vol. 28, No. 8, August 1990, pp. 1347-1352.

[19] Degani, D., and Levy, Y., "Asymmetric Turbulent Vortical Flows Over Slender Bodies," AIAA Paper No. 91-3296, 9th Applied Aerodynamics Conference, September 1991.

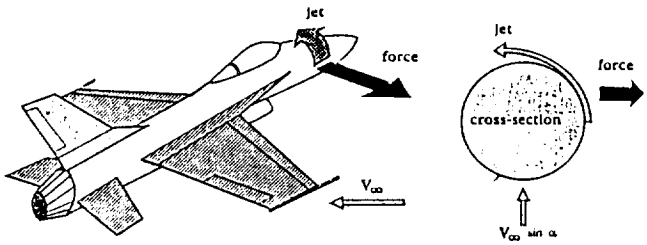

Fig. 1: Tangential blowing concept.

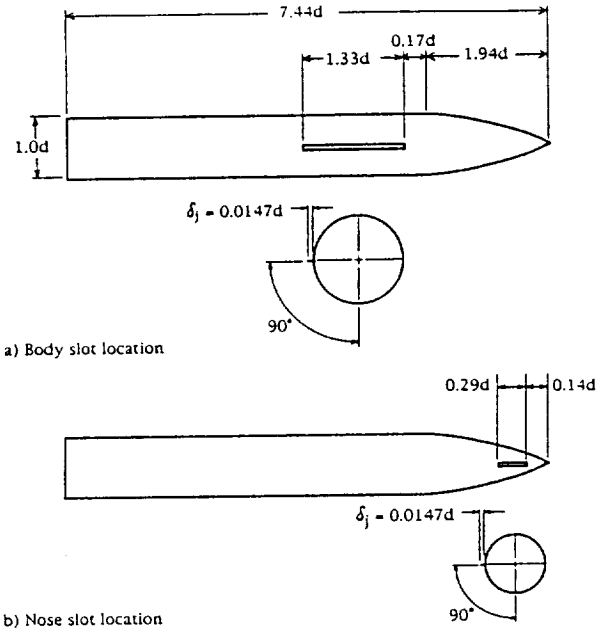

Fig. 2: Configurations under study.

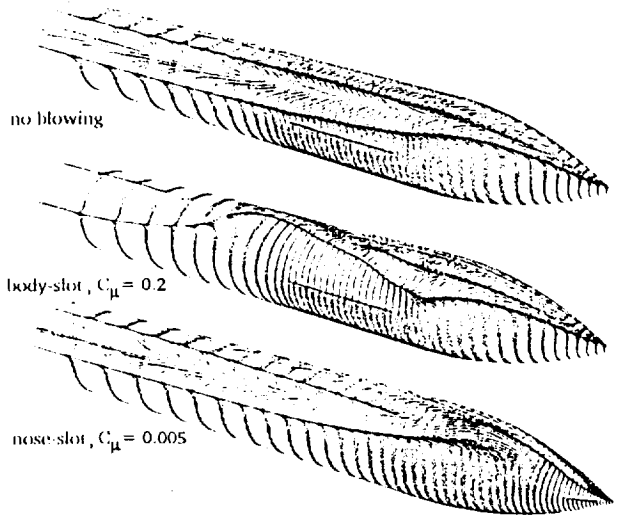

Fig. 3: Surface streamlines; α = 30 deg; Re_D = 5.2x10^4; M_∞ = 0.2.

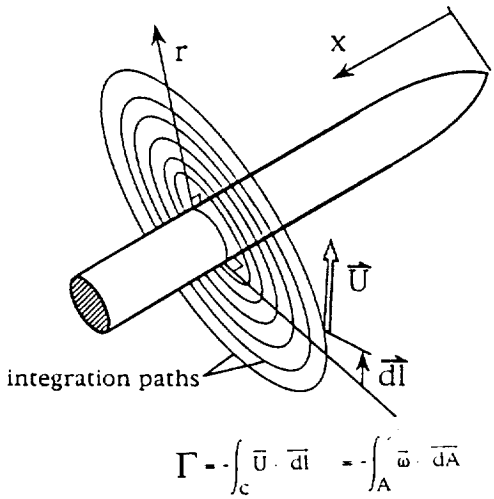

a) Integration paths at a typical x station.

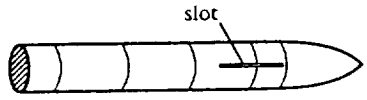

b) Body-slot stations on which integral is evaluated.

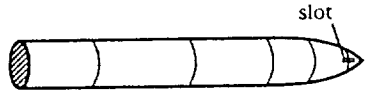

c) Nose-slot stations on which integral is evaluated.

Fig. 4: Circulation line integral paths.

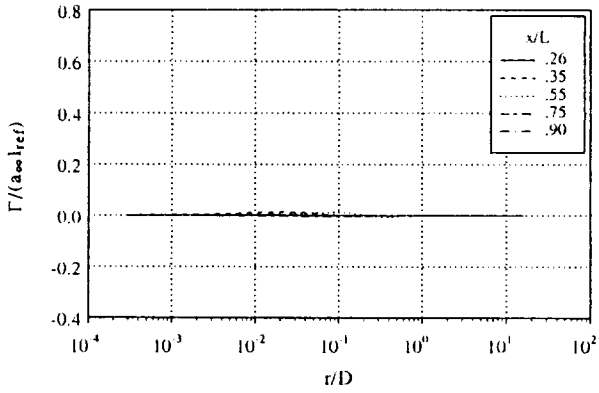

a) C_μ = 0.0

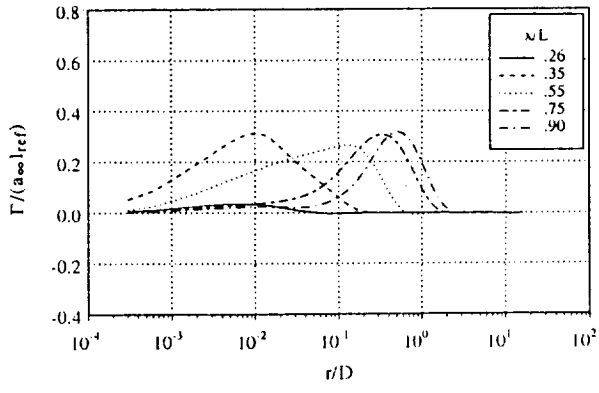

b) C_μ = 0.1

Fig. 5: Circulation distribution; α = 30 deg; Re_D = 5.2x10^4; M_∞ = 0.2.

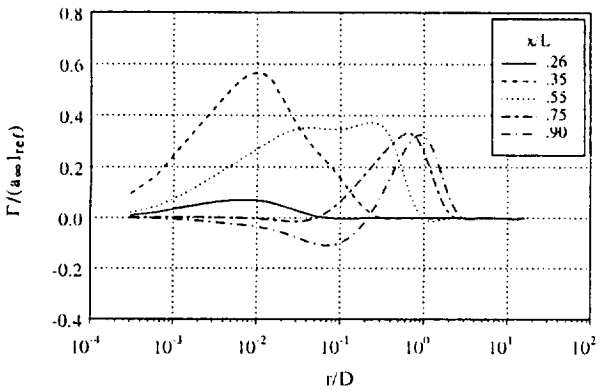

c) $C_\mu = 0.2$

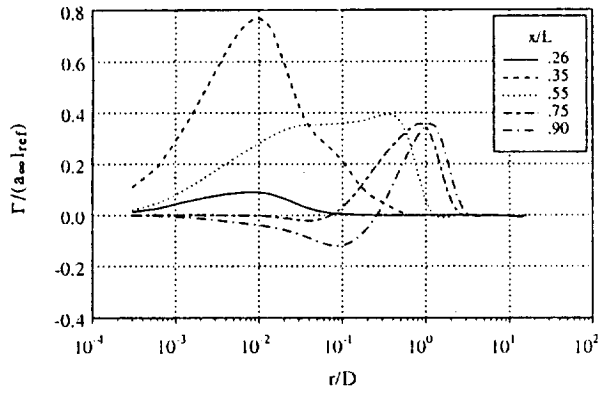

d) $C_\mu = 0.4$

Fig. 5: Circulation distribution; $\alpha = 30$ deg; $Re_D = 5.2\text{x}10^4$; $M_\infty = 0.2$. (continued)

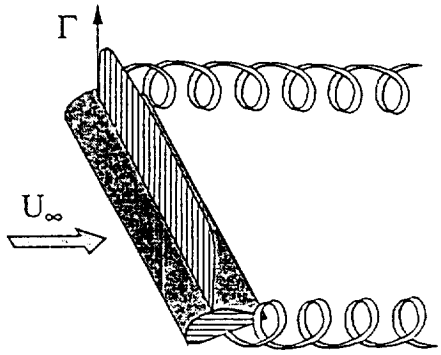

a) wing with near-constant lift distribution

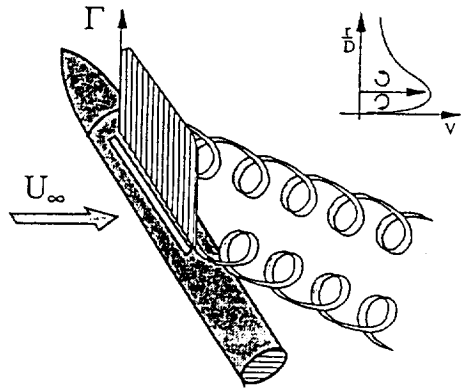

b) body with near-constant side force distribution

Fig. 6: Conceptual model for circulation induced by a tangential jet.

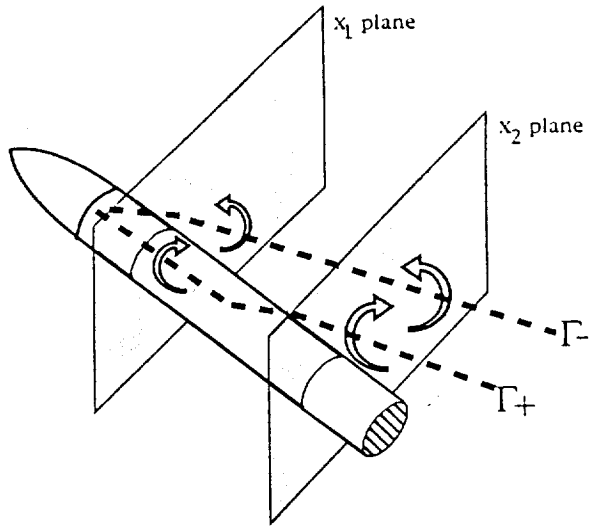

a) bound vortex model

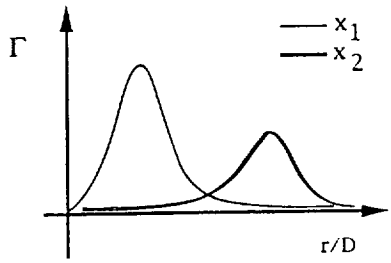

b) result of integration at two sample stations

Fig. 7: Expected result of summation of vorticty at different x stations with bound vortex model.

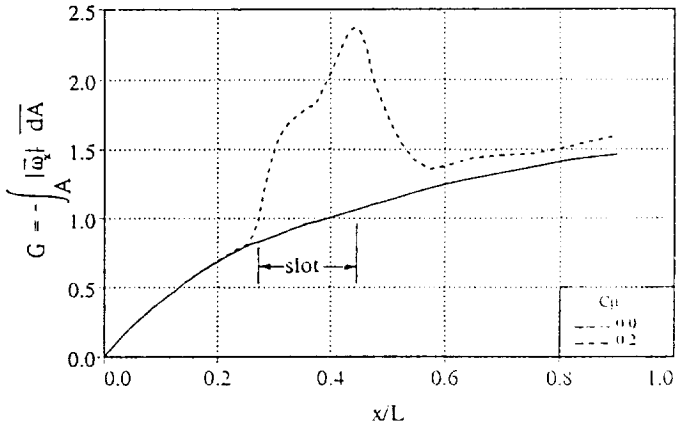

Fig. 8: Summation of absolute x vorticity in the flow field.

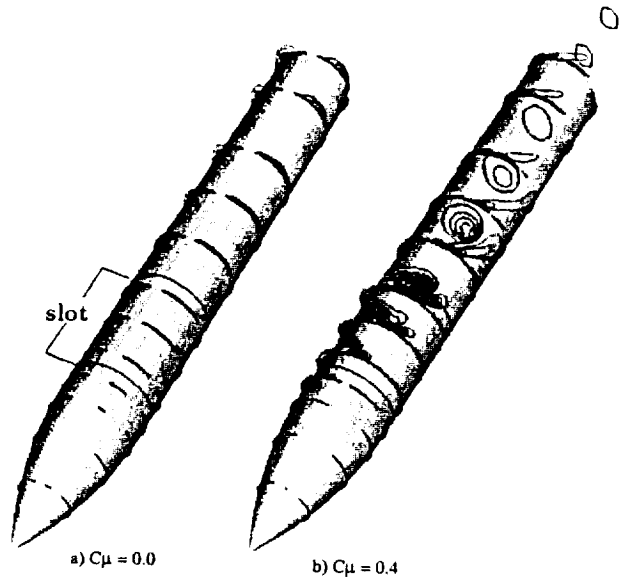

Fig. 9: Helicity density contours; α = 10 deg; Re_D = 5.2x10^4; M_∞ = 0.2.

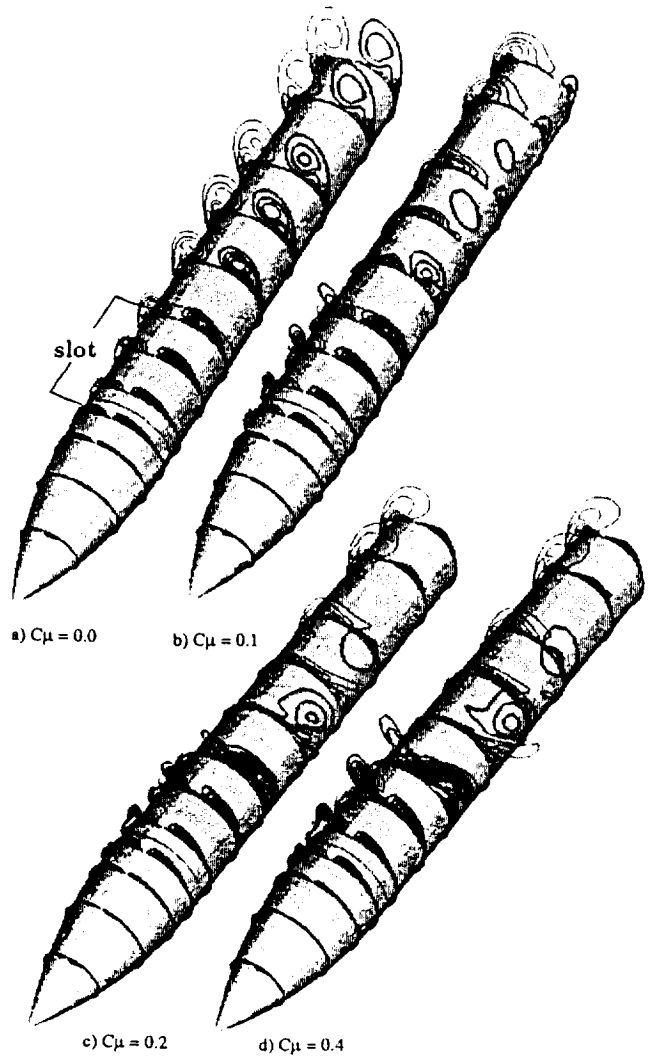

Fig. 10: Helicity density contours; α = 30 deg; Re_D = 5.2x10^4; M_∞ = 0.2.

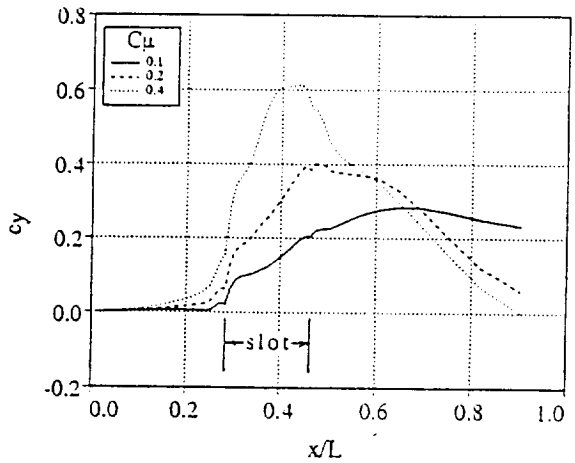

Fig. 11: Sectional side force; α = 30 deg; Re_D = 5.2x10^4; M_∞ = 0.2.

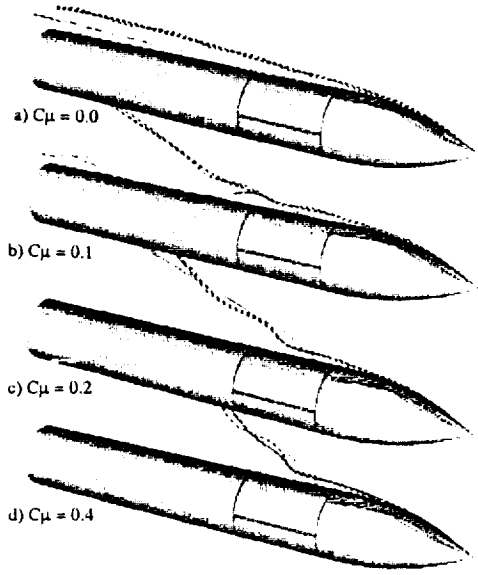

Fig. 12: Off-body particle traces; α = 30 deg; Re_D = 5.2x10^4; M_∞ = 0.2.

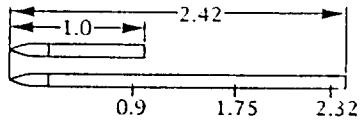

a) stations for circulation integration

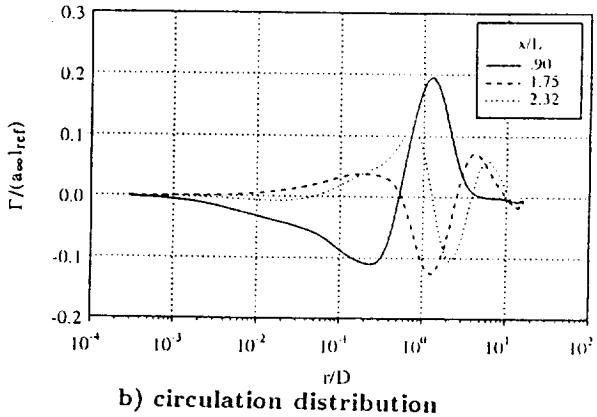

b) circulation distribution

Fig. 13: Circulation distribution and side force on an extended body; α = 30 deg; Re_D = 5.2x10^4; M_∞ = 0.2; C_μ = 0.4.

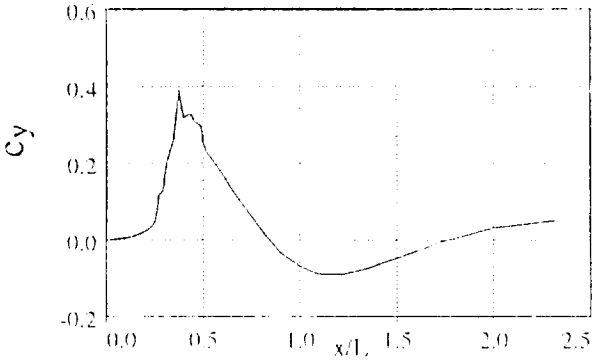

c) side force distribution

Fig. 13: Circulation distribution and side force on an extended body; α = 30 deg; Re_D = 5.2x10^4; M_∞ = 0.2; C_μ = 0.4 (continued).

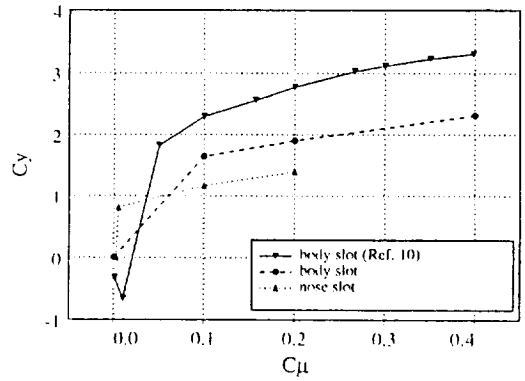

Fig. 14: Total side force for body and nose slot cases and experiment[10]; α = 30 deg; Re_D = 5.2x10^4; M_∞ = 0.2.

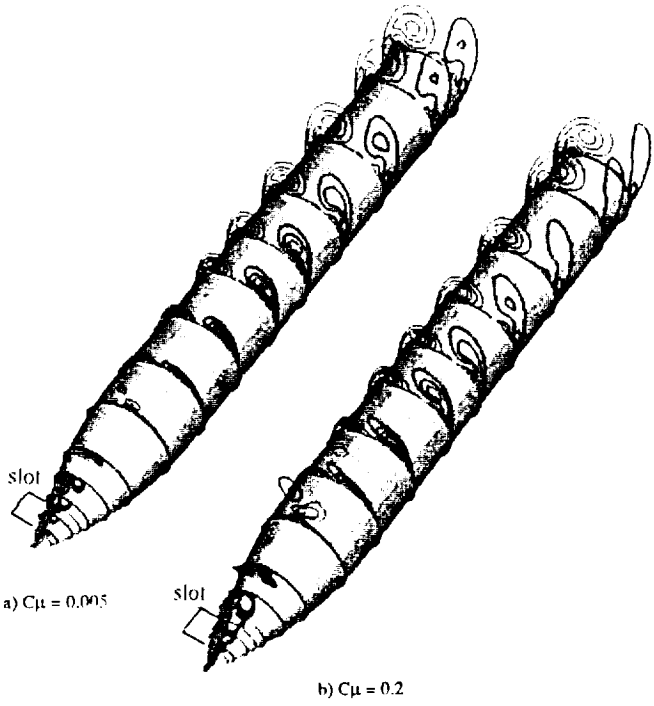

Fig. 15: Helicity density for nose-slot cases; α = 30 deg; Re_D = 5.2x10^4; M_∞ = 0.2.

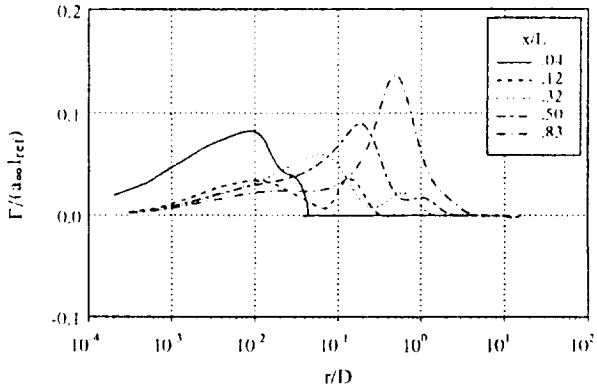

Fig. 16: Ciruclation distribution for nose-slot case; α = 30 deg; Re_D = 5.2x10^4; M_∞ = 0.2.

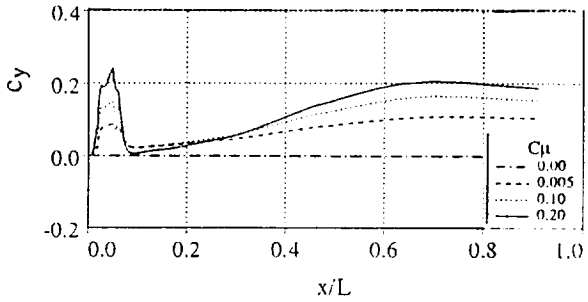

Fig. 17: Side force distribution one nose-slot case; α = 30 deg; Re_D = 5.2x10^4; M_∞ = 0.2; C_μ = 0.005.

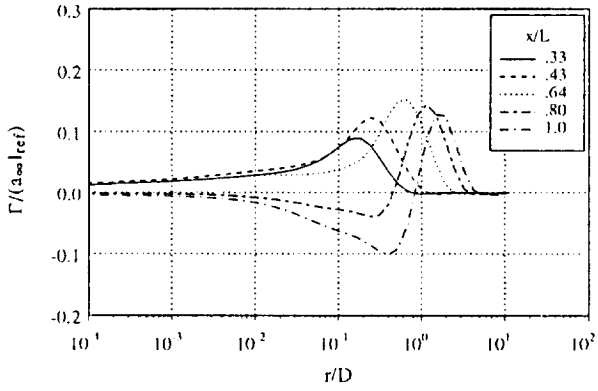

Fig. 18: Ciruclation distribution for body with geometric perturbation[19]; α = 30 deg; Re_D = 4.0x10^6; M_∞ = 0.2.

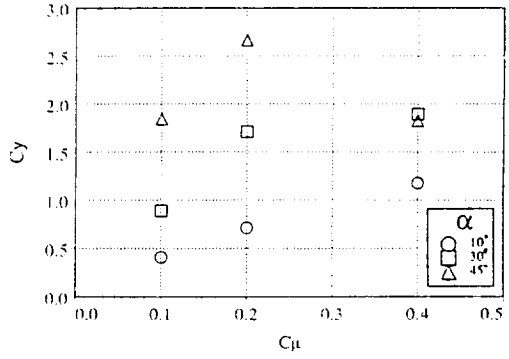

Fig. 19: Total side force for body-slot cases; Re_D = 5.2x10^4; M_∞ = 0.2.

APPENDIX B

AIAA-93-2961
Effects of Aft Geometry on Vortex Behavior and Force Production by a Tangential Jet on a Body at High Alpha

G. I. Font
MCAT Institute
Moffett Field, California

AIAA 24th
Fluid Dynamics Conference
July 6-9, 1993 / Orlando, FL

EFFECTS OF AFT GEOMETRY ON VORTEX BEHAVIOR AND FORCE PRODUCTION BY A TANGENTIAL JET ON A BODY AT HIGH ALPHA

G. I. Font*
MCAT Institute
Moffett Field, CA 94035

Abstract

Explored in this study are the physical effects of the numerical treatment of the aft geometry on the vortex behavior and force production due to a tangential jet on a body at a high angle of attack. The study is conducted numerically by solving the three-dimensional, compressible-flow, Reynolds-averaged Navier-Stokes equations. Two tangent-ogive cylinder configurations are used. The first configuration locates the computational exit plane at the end of the body, while the second caps the end of the body with a hemisphere and locates the exit plane far downstream. In both configurations, a blowing slot is located at the cylinder-ogive junction. Comparisons are made between results for the two configurations for cases with and without the jet present. Results indicate that inclusion of the wake of the body in the computations, while altering the flow in small details, does not change the character of the flow. The vortex behavior remains unaltered and the force distribution, while changing to some degree in magnitude, does not change in shape.

Nomenclature

C_n	normal force coefficient
c_n	sectional normal force coefficient: dC_n/dx
C_y	side force coefficient
c_y	sectional side force coefficient: dC_y/dx
$C\mu$	blowing momentum coefficient (see text)
D	cylinder diameter (see Fig. 1)
L_j	slot length (see Fig. 1)
M	Mach number
Re_D	Reynolds number, based on cylinder diameter
A_j	slot area, $\delta_j L_j$

*Research scientist, Member AIAA.

Nomenclature (continued)

A_{ref}	reference area, $L_j D$
V	flow velocity magnitude
α	angle of attack, degrees
δ_j	slot thickness (see Fig. 1)
ρ	density

Subscripts

D	based on cylinder diameter
j	jet
∞	freestream reference conditions

Introduction

The requirement of aircraft for higher levels of maneuverability has fostered numerous studies on improving their performance in the high angle of attack flight regime. Aircraft attempting to maneuver in this flight regime are prone to departure from controlled flight as their control surfaces become immersed in the flow separating from the fuselage and wings and lose effectiveness. The situation is exacerbated by the flow near the nose which tends to become asymmetric at high angles of attack, producing a side force that is destabilizing to the aircraft. Research into methods of correcting these problems has included studies where the flowfield near the nose is altered by pneumatic means[1-12] in an effort to either reduce the asymmetry or provide an additional side force that can be used to control the aircraft. Numerical treatment of this problem has often involved studies where the flow around an axisymmetric body is computed and where the body is extended to the computational exit plane.[7-12] This creates a non-physical situation where the influence of the wake from the body on the flow upstream is not taken into account. The present study is an attempt to ascertain the effects of the wake on one pneumatic control system: tangential slot-jet blowing.

In this study, computations are made for a body that extends to the computational exit plane and one in which the end of the body and wake are included. Comparisons are then made between the results of both types of computations at two angles of attack. This paper will show that inclusion of the body end and wake in the computations does not significantly change the physical character of the flow.

Present Work

The intention here is to study the effects of the numerical treatment of the aft end of a tangent-ogive cylinder on the flowfield characteristics and the side force produced by a tangentially blown slot-jet. The configuration under study is shown in Fig. 1. The model has a 1.94 caliber tangent ogive followed by a cylindrical section. Without the hemispherical end cap, the body is 7.44 calibers long. A jet slot is located on the cylindrical part of the body, immediately behind the ogive. The end of the cylinder is closed with a hemispherical cap.

Computations of the flow field around this configuration were carried out in two ways. In the first, the computational exit plane was placed at the end of the cylinder, at the hemisphere-cylinder junction. In the second, the computational exit plane was located twenty body diameters downstream from the end of the body. The grids for both configurations (shown in Fig. 2) are clustered near the surface and in the region of the slot. The grid with the flush exit plane contains 52, 100, and 60 points in the longitudinal, circumferential, and normal directions, respectively, while the grid with the far-field exit plane is 64 x 100 x 60. The y^+ at the first grid point off the surface is everywhere less than three, including the region where the jet is present.

The study is carried out numerically by solving the Reynolds-averaged, compressible-flow, thin-layer, Navier-Stokes equations. The code used to obtain the solution is F3D. It is well documented in the literature and further details may be found in Refs. 13-16. Solution is accomplished in a zonal manner. Communication between the zones is handled through a one-cell overlap where the cells match on a one-to-one basis. The zonal arrangement is shown in Fig. 3. The jet is implemented with an actuator plane method.[7] The longitudinal interface between zones in the slot region is utilized to introduce the jet into the computation as an actuator plane boundary condition.

The turbulence model for the boundary layers is the Baldwin-Lomax[16] model with Degani-Schiff modifications.[17] The turbulence model for the jet was developed by Roberts.[18] The turbulence model for the boundary layers was included when experiments showed turbulent behavior in the boundary layers in the jet and aft of the slot, while blowing was present.[11]

The boundary condition implemented on the numerical exit plane is a zeroth order extrapolation. The same exit boundary condition was employed for both configurations, the only difference being the location of the exit plane. In the case of the capped body, the exit plane is defined as those stations that fall within a 50 deg. ray extended back from the tip of the nose with 0 deg. defined as the longitudinal axis. This was done in order to assure that no gradients existed between the region where the extrapolation was in effect and the region where the outer boundary was held at free stream conditions. Computations were carried out with the exit plane at larger distances from the body and no changes were found in the results.

The flow conditions for the present study are as follows: the angles of attack used are 30 and 45 deg., the Mach number is 0.2 and the Reynolds number, based on freestream conditions and cylinder diameter, is 52000. These conditions were chosen to facilitate comparison with previous studies.[4,10-12]

Results

α = 30 deg, no blowing

Figure 4 displays the surface streamlines and the off-body particle traces for both bodies where no blowing is present and the angle of attack is 30 deg. In the following discussion, the case where the end of the body and wake is included in the computation will be referred to as the "capped" body. The case where the computational exit plane is placed flush with the end of the cylinder will be referred to as the "flush-exit" body. The separation pattern along most of the body is identical for the two cases. Differences occur only near the end of the body where, for the case where the end of the body is included in the computation, the skin-friction lines, including the primary and secondary separation lines, must end at singular points on the hemispherical cap. Off-body particle traces, also shown in Fig. 4, indicate the vortex trajectories. The vortex of one side of the body is denoted with solid lines while the vortex on the other side is denoted with dashed lines. For both cases, the vortices are symmetrically located on the leeside of the body. Their distance from the surface at any point along the body is not significantly affected by the inclusion of the wake in the computation. The vortices in the capped body computation begin to align with the onset flow aft of the end of the body.

Figure 5 shows the total vorticity magnitude at two stations along the body. The first station is near the beginning of the cylindrical part of the body, at x/D = 2.8. The second station is near the end of the body, at x/D = 6.1. At both stations, the vorticity magnitude and position of maximum vorticity is in good agreement between the two cases indicating that the influence from the aft end geometry is minor.

Figure 6 shows the normal force distribution for the cases in which no jet was present. Only stations upstream of the hemispherical end cap are shown. The

normal force is the same for both bodies over the forward portion of the body. The normal force for the capped body is slightly lower in the aftbody at nearly all stations.

α = 30 deg, blowing present

The cases where the tangential slot jet was present in the computation will now be discussed. The jet momentum ratio, defined as,

$$C_\mu = \frac{\rho_j V_j^2 A_j}{\rho_\infty V_\infty^2 A_{ref}}$$

was 0.2 providing a jet exit velocity of $M_j = 0.5$. In this expression, A_j is the slot area and A_{ref} is the slot length multiplied by the diameter of the body. Figure 7 shows the surface streamlines and off-body particle traces for the cases with a tangential jet present. The surface streamline pattern for both cases is similar in the nose and aft body regions. The off-body particle traces show that the vortex behavior is changed somewhat by the inclusion of the wake in the computation. The slot-side vortex for the capped body computation, while lifting from the body at the same location as in the flush-exit computation, remains closer to the body. Part of the reason for this effect is that the jet does not separate at the same location for both cases. In the capped body case, the jet remains attached farther over the top of the body in the forward part of the slot, as seen in Fig. 8, where the surface streamlines are viewed from above. The trajectory of the vortex on the side of the body opposite slot (dashed traces) does not change with the change in the position of the exit plane.

The vorticity magnitude contours for the blowing cases and α = 30 deg. are shown in Fig. 9. Because the jet remains attached longer for the capped body case, the jet-provided vorticity has greater interaction with the vortex opposite the slot. Consequently, the vorticity magnitude patterns are very different between the two cases at station 1, in the slot region. Downstream of the slot, however, the vorticity magnitude pattern is negligibly different between the two cases. The vortex that lifts off the surface on the slot side (solid lines in Fig. 7) is not resolved in the vorticity magnitude calculations. (It should appear to the left, as viewed, of the high vortex.) This is because the vortex left the body near the nose and, consequently, does not carry as much vorticity as its counterpart on the other side of the body. This, combined with the relative coarseness of the grid at that distance from the body, make the gradients too small to resolve the vorticity.

The side and normal force distributions for the blowing cases are shown in Fig. 10. A large normal force is created in the slot region (Fig. 10a) due to the suction created by the jet as it remains attached over the leeside of the body. The normal force distribution for both cases closely resemble each other in magnitude as well as in shape. Over most of the aftbody, the force produced by the jet in the capped body case is lower than the force produced in the flush-exit case. The normal force for both cases is larger than the force resulting in the no-blowing computations (Fig. 6). The side force distribution is shown in Fig. 10b. The shape and magnitude, as with the normal force, does not differ greatly between the two cases. The body where the end is included in the computation produces a greater side force in the slot region due to the jet remaining attached to the surface longer. Downstream of the slot, however, this case produces a smaller side force. The side force levels remain close to within one body diameter of the rear of the cylinder.

α = 45 deg, no blowing

Figure 11 displays the surface streamlines and the off-body particle traces for the no-blowing cases where α = 45 deg. The surface streamlines for the capped body and the flush-exit body are virtually identical over the cylindrical part of the body. The off-body particle traces are also very similar. The only differences manifest themselves after the hemisphere/cylinder junction where the vortices of the capped body turn upward. Figure 12 shows the total vorticity magnitude contours for these cases. At station 1, the treatment of the aft end of the body does not appear to change the solution. Closer to the aft end (station 2), however, the vortices of the capped body are weaker. This leads to lower suction on the leeside of the body and, consequently, lower normal force levels in the aftbody as shown in the normal force distribution displayed in Fig. 13. The weaker vortices and lower suction on the capped computation are analogous to the effects observed when a 2D cylinder is compared to a sphere of equal diameter. Perhaps the three dimensional nature of the capped body is providing a mechanism for pressure relief.

α = 45 deg, blowing present

Figure 14 shows the surface streamlines and off-body particle traces for the blowing cases where the angle of attack is 45 deg. The jet momentum coefficient, $C\mu$, is also 0.2. In the forward part of the body, the separation line patterns are very similar for the two cases. Aft of the slot, some differences are observed in the location of the secondary separation lines. The off-body particle traces show no differences in the vortex trajectories for the two cases. Figure 15 displays the total vorticity magnitude contours. In the slot region, the two cases are not significantly different. In the aftbody, however, while the vortex orientation is the same, the vortex strengths of the capped body are, again,

lower. The difference in strength is probably responsible for the differences in the secondary separation pattern observed in the aftbody in Fig. 14.

The sectional force distributions for the blowing cases are shown in Fig. 16. The normal force in the slot region decreases for both cases when compared to the no-blowing computations. This is because the jet does not remain attached for a significant distance over the leeside of the body. Thus, while the jet does not create significant suction over the leeside of the body, it does move the position of separation toward the leeside of the body enough to reduce the normal force. In the aftbody, the normal force does increase to levels higher than observed in the no-blowing cases. The flush-exit computation, again, produced higher force levels than the computation with capped body. The side force distributions are shown in Fig. 16b. The shapes of the distributions for both cases are very similar to each other until about x/D = 6.5. However, the side force is significantly lower for the capped body than for the flush-exit body over the entire aftbody.

Conclusions

A numerical study has been conducted exploring the effects on vortex behavior and side force production of a tangential jet subject to the inclusion of the aft end of the body and wake in the computations. Results indicate that inclusion of the wake of the body in the computations, while altering the flow in details, does not change the physical character of the flow. The flow features of the computation that placed the numerical exit plane at the end of the cylinder of the body are comparable to within one diameter of the end of the body to those of computations that moved the exit plane to the far-field. The force distributions, while being similar for the two cases, were generally lower in the aftbody for the case where the end of the body was included. This was probably due to the lower vortex strengths observed in the aft end of the capped body cases, especially at the higher angle of attack. The differences between results for the two cases diminished with decreasing angle of attack.

Acknowledgements

The author would like to thank Drs. Lewis Schiff, David Degani and Murray Tobak for their many helpful discussions. This work was supported by NASA Grant NCC 2-729.

References

1. Moore, W. A., Skow, A. M. and Lorinez, D. J., "Enhanced Departure/Spin Recovery of Fighter Aircraft Through Control of the Forebody Vortex Orientation," AIAA Paper No. 80-0173, AIAA 18th Aerospace Sciences Meeting, January 1980.

2. Peake, D. J., Owen, F. K., and Johnson, D. H., "Control of Forebody Vortex Orientation to Alleviate Side Forces," AIAA Paper No. 80-0183, AIAA 18th Aerospace Sciences Meeting, January 1980.

3. Malcolm, G. N., Ng, T. T. and Murri, D. G., "Development of Non-conventional Control Methods for High Angle of Attack Flight Using Vortex Manipulation," AIAA Paper No. 89-2192, 27th Aerospace Sciences Meeting, January 1989.

4. Celik, Z. Z. and Roberts, L., "Vortical Flow Control on a Slender Body at High Angles of Attack" AIAA 91-2868, Atmospheric Flight Mechanics Conference, August 1991.

5. Ng, T. T., and Malcolm, G. N., "Aerodynamic Control Using Forebody Blowing and Suction," AIAA Paper No. 91-0619, 29th Aerospace Sciences Meeting, January 1991.

6. Rosen, B. S. and Davis, W. H., "Numerical Study of Asymmetric Air Injection to Control High Angle-of-attack Forebody Vortices on the X-29 Aircraft," AIAA Paper No. 90-3004-CP, 1990

7. Tavella, D. A., Schiff, L. B. and Cummings, R.,"Pneumatic Vortical Flow Control at High Angles of Attack," AIAA Paper No. 90-0098, 28th Aerospace Sciences Meeting, January 1990

8. Gee, K., Tavella, D. A. and Schiff, L. B., "Computational Optimization of a Pneumatic Fuselage Forebody Flow Control Concept," AIAA Paper No. 91-3249, 9th Applied Aerodynamics Conference, September 1991.

9. Degani, D., "Numerical Investigation of the Origin of Vortex Asymmetry," AIAA Paper No. 90-0593, AIAA 28th Aerospace Sciences Meeting, January 1990.

10. Font, G. I., and Tavella, D. A., "High Alpha Aerodynamic Control by Tangential Fuselage Blowing," *AIAA Journal*, Vol. 30, No. 5, May 1992, pp. 1321-1330.

11. Font, G. I., Celik, Z. Z., and Roberts, L. "A Numerical and Experimental Study of Tangential Jet Blowing Applied to Bodies at High Angles of Attack,"

AIAA Paper No. 91-3253, 9th Applied Aerodynamics Conference, September 1991.

12. Font, G. I., "Force Production Mechanisms of a Tangential Jet on Bodies at High Alpha.," AIAA Paper No. 92-4648, Atmospheric Flight Mechanics Conference, August 1992.

13. Steger, J. L., Ying, S. X., and Schiff, L. B., "A Partially Flux-Split Algorithm for Numerical Simulation of Unsteady Viscous Flows," Proceedings of a Workshop on Computational Fluid Dynamics, University of California, Davis, 1986.

14. Ying, S. X., "Three-Dimensional Implicit Approximately Factored Schemes for Equations in Gasdynamics," Ph.D. Thesis, Stanford University,1986 (also SUDAAR 557, June 1986).

15. Ying, S. X., Baganoff, D., Steger, J. L., and Schiff, L. B., "Numerical Simulation of Unsteady, Viscous, High-Angle-of-Attack Flows Using a Partially Flux-Split Algorithm," AIAA Paper 86-2179-CP, AIAA Atmospheric Flight Mechanics Conference, Aug. 1986.

16. Baldwin, B.S., and Lomax, H., "Thin Layer Approcimation and Algebraic Model for Separated Turbulent Flows," AIAA paper 78-257, AIAA 16th Aerospace Sciences Meeting, January 1978.

17. Degani, D., and Schiff, L.B., "Computation of Turbulent Supersonic Flows Around Pointed Bodies Having Crossflow Separation," *Journal of Computational Physics*, Vol. 66 (1986), pp. 173-196.

18. Roberts, L., "A Theory for turbulent Curved Wall Jets," AIAA Paper No. 87-0004, 1987.

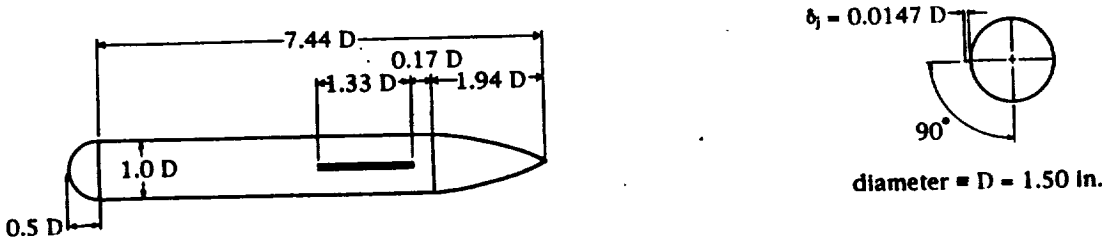

Fig. 1: Configuration under study.

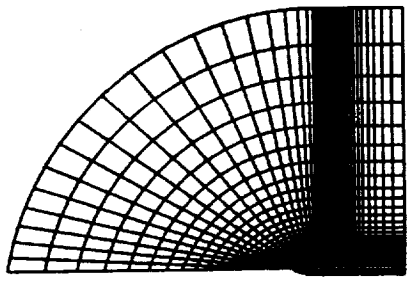

a) body with exit plane flush

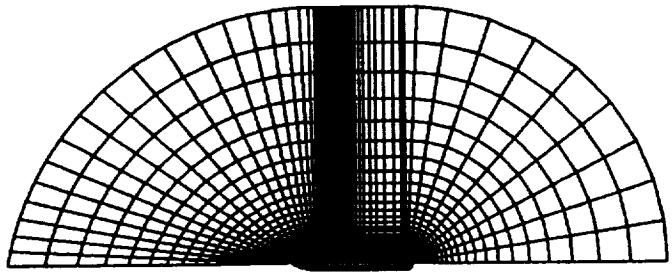

b) body with exit plane in far-field

Fig. 2: Computational Grids.

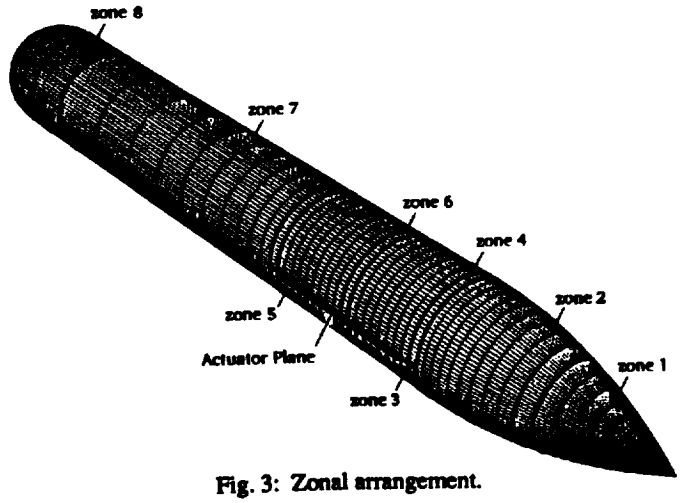

Fig. 3: Zonal arrangement.

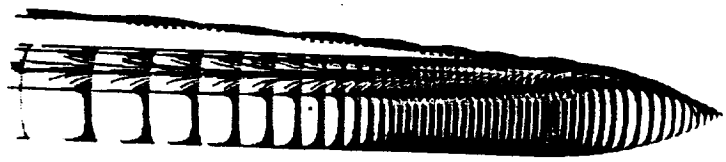

a) body with flush exit plane

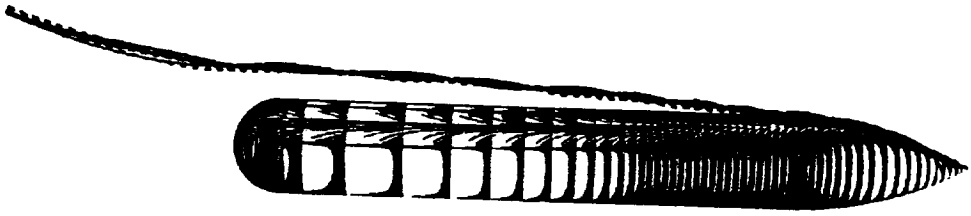

b) body with far-field exit plane

Fig. 4: Surface streamlines and off-body particle traces;
$\alpha = 30$ deg; $Re_D = 5.2 \times 10^4$; $M_\infty = 0.2$; no blowing.

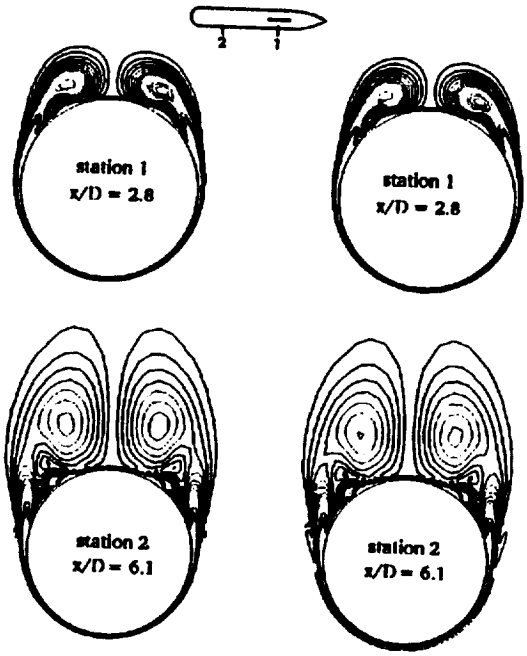

a) body with flush exit plane b) body with far-field exit plane

Fig. 5: Vorticity magnitude contours;
$\alpha = 30$ deg; $Re_D = 5.2 \times 10^4$; $M_\infty = 0.2$; no blowing.

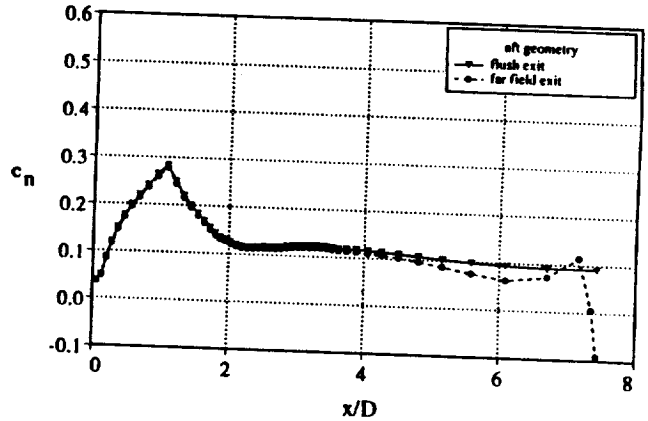

Fig. 6: Normal force distribution;
$\alpha = 30$ deg; $Re_D = 5.2 \times 10^4$; $M_\infty = 0.2$; no blowing.

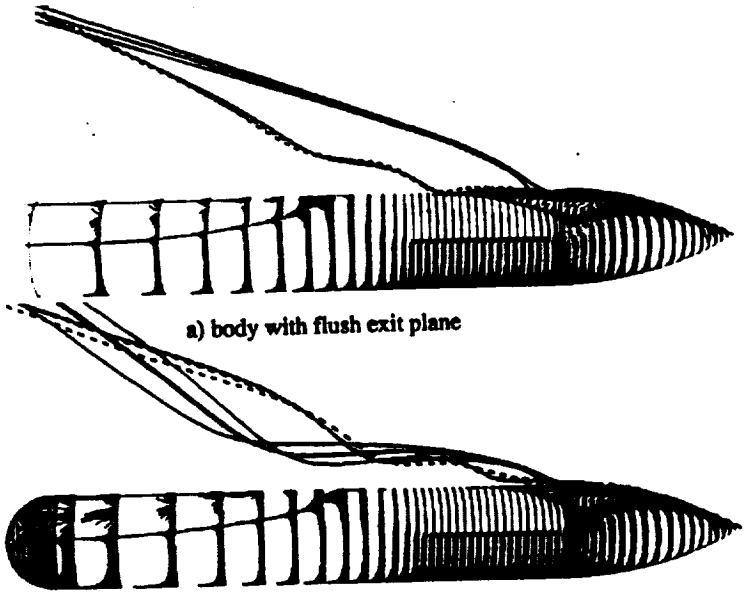

a) body with flush exit plane

b) body with far-field exit plane

Fig. 7: Surface streamlines and off-body particle traces with blowing present; $\alpha = 30$ deg; $Re_D = 5.2 \times 10^4$; $M_\infty = 0.2$; $C\mu = 0.2$.

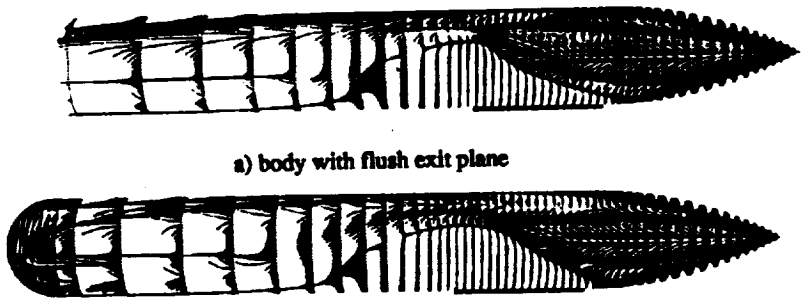

a) body with flush exit plane

b) body with far-field exit plane

Fig. 8: Surface streamlines (top view) with blowing present; $\alpha = 30$ deg; $Re_D = 5.2 \times 10^4$; $M_\infty = 0.2$; $C\mu = 0.2$.

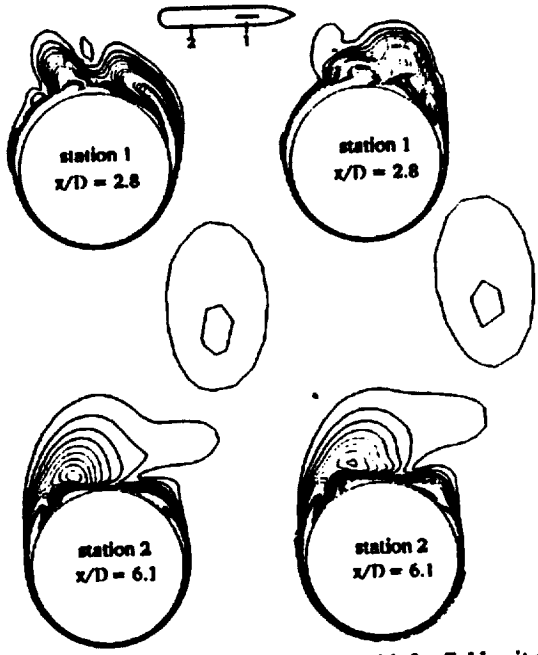

a) body with flush exit plane b) body with far-field exit plane

Fig. 9: Vorticity magnitude contours with blowing present; $\alpha = 30$ deg; $Re_D = 5.2 \times 10^4$; $M_\infty = 0.2$; $C\mu = 0.2$.

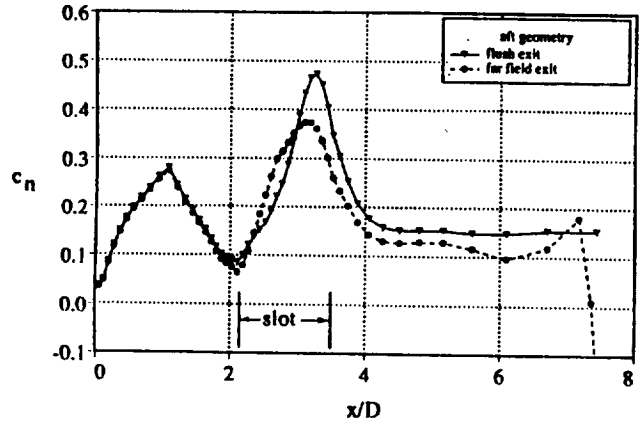

a) normal force distribution

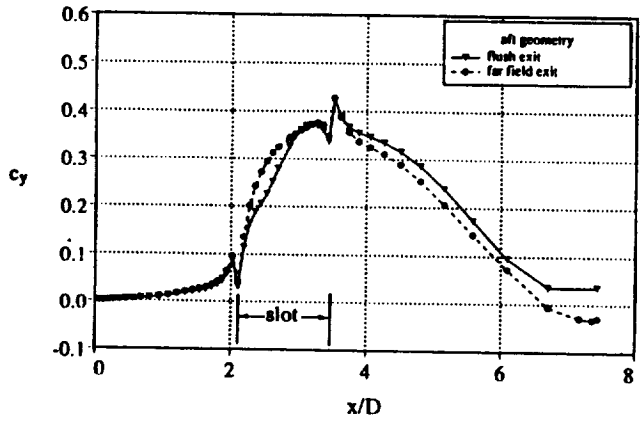

b) side force distribution

Fig. 10: Force distributions with blowing present;
α = 30 deg; $Re_D = 5.2 \times 10^4$; $M_\infty = 0.2$; C_μ=0.2.

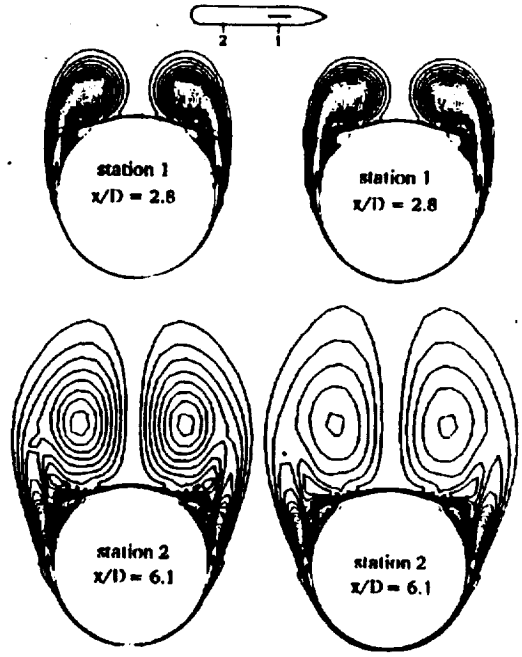

a) body with flush exit plane b) body with far-field exit plane

Fig. 12: Vorticity magnitude contours;
α = 45 deg; $Re_D = 5.2 \times 10^4$; $M_\infty = 0.2$; no blowing.

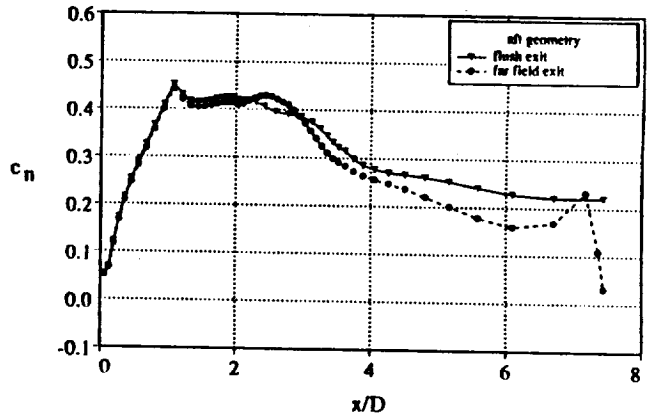

Fig. 13: Normal force distribution;
α = 45 deg; $Re_D = 5.2 \times 10^4$; $M_\infty = 0.2$; no blowing.

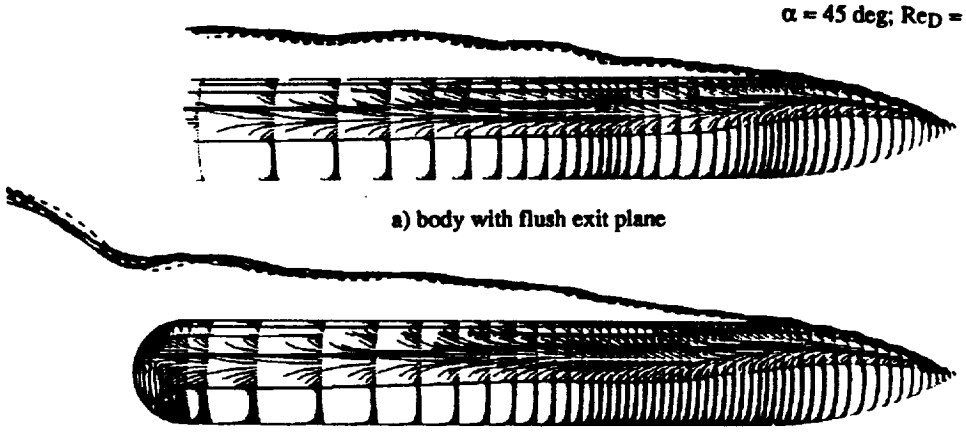

a) body with flush exit plane

b) body with far-field exit plane

Fig. 11: Surface streamlines and off-body particle traces;
α = 45 deg; $Re_D = 5.2 \times 10^4$; $M_\infty = 0.2$; no blowing.

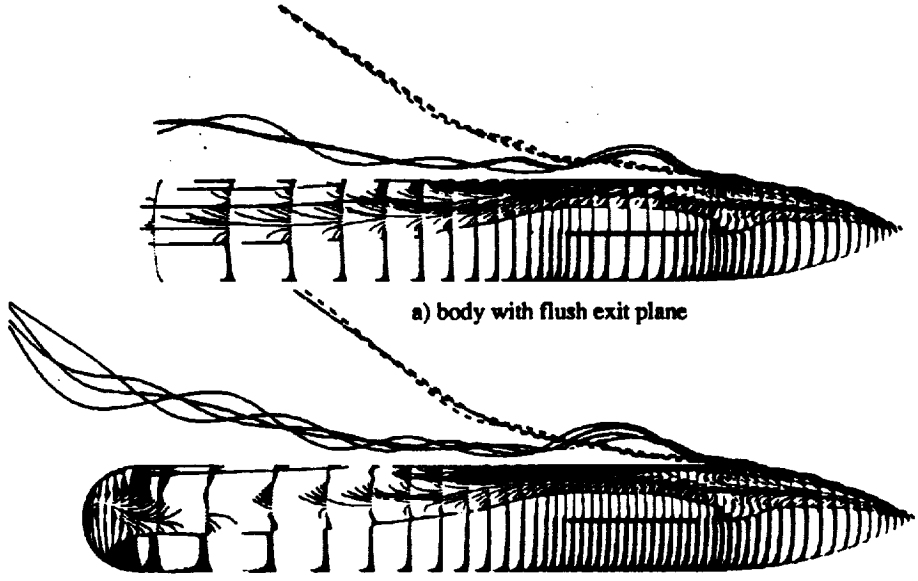

a) body with flush exit plane

b) body with far-field exit plane

Fig. 14: Surface streamlines and off-body particle traces with blowing present; α = 45 deg; $Re_D = 5.2 \times 10^4$; $M_\infty = 0.2$; $C\mu$=0.2.

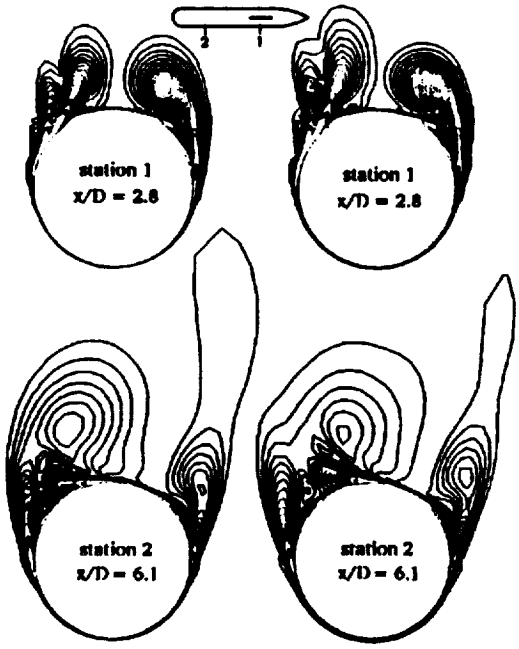

a) body with flush exit plane b) body with far-field exit plane

Fig. 15: Vorticity magnitude contours with blowing present; α = 45 deg; $Re_D = 5.2 \times 10^4$; $M_\infty = 0.2$; $C\mu$=0.2.

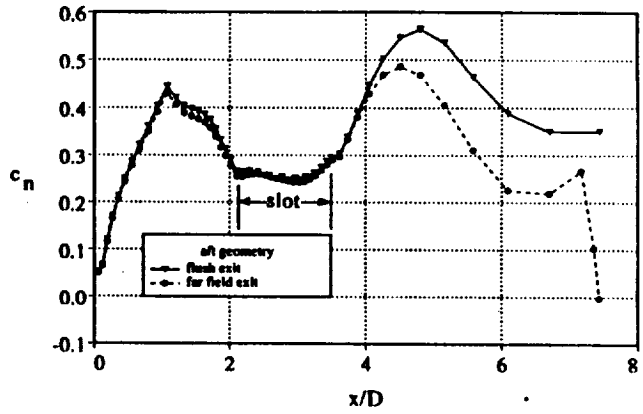

a) normal force distribution

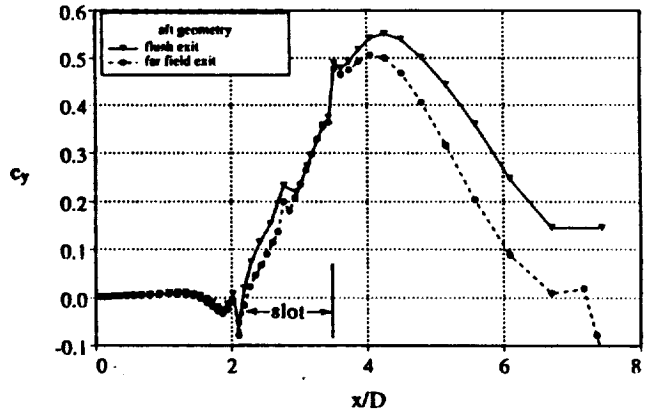

b) side force distribution

Fig. 16: Force distributions with blowing present; α = 45 deg; $Re_D = 5.2 \times 10^4$; $M_\infty = 0.2$; $C\mu$=0.2.

APPENDIX C

NUMERICAL FRAMEWORK FOR ANALYZING FLOW SENSITIVITY TO SMALL CHANGES

G. I. Font
MCAT Institute
Moffett Field, CA 94035

D. C. Hill
Center for Turbulence Research
Stanford, CA 94305

Abstract

The solution of the equations adjoint to the Navier-Stokes equations provide a means to explore the flow field sensitivity to a small changes. This allows the optimization of the design of a flow control configuration. This work develops the formulation necessary to numerically solve the adjoint set of equations. It explores the computational issues involving discretization, coordinate transformation, flux linearization, factorization, and implicit formulation of the adjoint set of equations.

Introduction

High speed civil transports, whether supersonic or hypersonic, must land and take off at high angle of attack because of their highly swept wings. Aircraft attempting to maneuver in this flight regime are prone to departure from controlled flight as their control surfaces lose effectiveness when becoming immersed in the flow separating from the fuselage and wings. The situation is exacerbated by the flow near the nose which tends to become asymmetric at high angle of attack, producing a side force which is destabilizing to the aircraft. One method of correcting these problems is to alter the flow field near the nose by pneumatic means in an effort to either reduce the asymmetry or provide an additional side force which can be used to control the aircraft. Traditionally, analysis of these control methods involves multiple computations of a single flow field subject to a

single pneumatic perturbation in an effort to "map" the effectiveness of the control methods. The intricate nature of the three-dimensional flow dynamics means that this map does not have an obvious form. Researchers are led to perform repeated computations for different levels and physical configurations of the perturbation. Consequently, the assessment of the effectiveness of any control method by this means is prohibitively expensive.

The aim of the present work is to present an alternative strategy to that described above for finding effective control configurations by direct computation. The present scheme makes use of the solution to the adjoint to the linearized Navier-Stokes equations. This solution plays an integral role in the search for an optimal configuration.

The solution to the adjoint linearized Navier-Stokes equations, subject to carefully chosen boundary conditions, provides a description of the sensitivity of the flow field to a general perturbation. The adjoint field, obtained by a *single* computation, maps the effectiveness of *any* control configuration upon a quantity such as, for example, drag, provided the control force is sufficiently small. The interpretation of the adjoint field is straight forward: If the adjoint field is very large at some point in the flow, then the application of even a small control force will give rise to a large response. On the other hand, if the adjoint field is very small even large quantities of control will have very little effect.

The examination of the linear sensitivity is not a restriction. In the language of optimal control theory, the adjoint solution defines the functional derivative of the drag with respect to changes in the control configuration. Our adjoint solution defines a "steepest-descent" direction by which a search may be conducted for optimal solutions of a configuration which can involve large amounts of control (see Ref. 1).

The idea of optimization in fluid mechanics is certainly not new. To date most efforts at optimization have involved inviscid calculations, and aimed at minimizing form drag (Ref. 2). Alternatively, airfoil sections have been designed based on the desire for a particular surface pressure distribution (Ref. 3). In the present work the sensitivity of solutions to the full Navier-Stokes equations are being investigated. The non-self-adjoint nature of the governing equations raises new issues in both theory and computation. Solution of the adjoint equations have been obtained using spectral methods. These solutions, however, were limited to configurations which could be described analytically

and 2-dimensional flow fields (Ref. 4). In an effort to extend the method to non-analytical configurations, a finite difference approach will be adopted for the solution of the adjoint equations. The method lends itself to extension into 3-Dimensional computations although the present work will be limited to 2D.

The present work starts the numerical formulation from the adjoint set of equations first set forth by Ref. 4. This work develops the framework necessary to numerically solve the adjoint set of equations. It explores the computational issues involving discretization, coordinate transformation, flux linearization, factorization, and implicit formulation of the adjoint set of equations.

Numerical Formulation

The set of equations which is adjoint to the compressible Navier-Stokes equations was first set forth by Ref. 4 as:,

$$\frac{\partial u}{\partial t}+\left(2\overline{U}\frac{\partial u}{\partial x}+\overline{V}\frac{\partial v}{\partial x}+\frac{1}{\mathrm{Re}}\frac{\partial^2 u}{\partial x^2}+\frac{\partial P}{\partial x}\right)+\left(\overline{V}\frac{\partial u}{\partial y}+\frac{1}{\mathrm{Re}}\frac{\partial^2 u}{\partial y^2}\right)=0 \tag{1a}$$

$$\frac{\partial v}{\partial t}+\left(\overline{U}\frac{\partial v}{\partial x}+\frac{1}{\mathrm{Re}}\frac{\partial^2 v}{\partial x^2}\right)+\left(\overline{U}\frac{\partial u}{\partial y}+2\overline{V}\frac{\partial v}{\partial y}+\frac{1}{\mathrm{Re}}\frac{\partial^2 v}{\partial y^2}+\frac{\partial P}{\partial y}\right)=0 \tag{1b}$$

$$\frac{\partial u}{\partial x}+\frac{\partial v}{\partial y}=0 \tag{1c}$$

Note that the pressure does not exist explicitly in any of the governing equations. This is a consequence of using the incompressible formulation for the Navier-Stokes equations as the starting point for the derivation of the adjoint set. To establish the actual adjoint pressure a Poisson problem must be solved. Alternatively, the concept of pseudo-compressibility can be employed. For a flow in which only the steady state is sought, the continuity equation can be modified to include the pressure explicitly:[5]

$$\frac{1}{\beta^2}\frac{\partial P}{\partial t}+\nabla\cdot\vec{u}=0 \tag{2}$$

The parameter β represents the artificial speed of sound. The pressure term vanishes when the solution converges, therefore, the final solution does not violate continuity. The modified continuity equation becomes,

$$\frac{\partial P}{\partial t}+\beta^2\frac{\partial u}{\partial x}+\beta^2\frac{\partial v}{\partial y}=0 \tag{3}$$

Equation (3) replaces 1c as part of the governing equation set. The governing equations can now be concisely written as,

$$\frac{\partial \vec{a}}{\partial t}+\overline{\overline{G}}\frac{\partial \vec{a}}{\partial x}+\frac{1}{\mathrm{Re}}\frac{\partial \vec{b}}{\partial x}+\overline{\overline{H}}\frac{\partial \vec{a}}{\partial y}+\frac{1}{\mathrm{Re}}\frac{\partial \vec{c}}{\partial y}=0 \tag{4a}$$

where the vectors and tensors have the following components,

$$\vec{a} = \begin{bmatrix} u \\ v \\ P \end{bmatrix}, \qquad \vec{b} = \begin{bmatrix} \frac{\partial u}{\partial x} \\ \frac{\partial v}{\partial x} \\ 0 \end{bmatrix}, \qquad \vec{c} = \begin{bmatrix} \frac{\partial u}{\partial y} \\ \frac{\partial v}{\partial y} \\ 0 \end{bmatrix} \tag{4b}$$

$$\overline{\overline{G}} = \begin{bmatrix} 2\overline{U} & \overline{V} & 1 \\ 0 & \overline{U} & 0 \\ \beta^2 & 0 & 0 \end{bmatrix}, \qquad \overline{\overline{H}} = \begin{bmatrix} \overline{V} & 0 & 0 \\ \overline{U} & 2\overline{V} & 1 \\ 0 & \beta^2 & 0 \end{bmatrix} \tag{4c}$$

Here, $\overline{\overline{G}}$ and $\overline{\overline{H}}$ are functions of space but are constant in time.

Coordinate Transfer

Solving the adjoint set on a non-analytical geometry will require the equations to be recast into a general, preferably a body-conforming, coordinate system. The mapping from a two-dimensional cartesian system (x,y) into a general system (ξ,η) is defined as follows:

$$\xi = \xi(x,y)$$
$$\eta = \eta(x,y)$$

The transformation is standard and the resulting metrics are,

$$\xi_x = J(y_\eta),\ \ \xi_y = -J(x_\eta),\ \ \eta_x = -J(y_\xi),\ \ \eta_y = J(x_\xi) \tag{5}$$

where the jacobian of the transformation is,

$$J = \left(x_\xi y_\eta - x_\eta y_\xi\right)^{-1} \tag{6}$$

Applying the chain rule to the governing equations (4) gives:

$$\frac{1}{J}\frac{\partial \vec{a}}{\partial t} + \overline{\overline{G}}\frac{1}{J}\left\{\frac{\partial \vec{a}}{\partial \xi}\frac{\partial \xi}{\partial x}+\frac{\partial \vec{a}}{\partial \eta}\frac{\partial \eta}{\partial x}\right\} + \frac{1}{\mathrm{Re}}\frac{1}{J}\left\{\frac{\partial \vec{b}}{\partial \xi}\frac{\partial \xi}{\partial x}+\frac{\partial \vec{b}}{\partial \eta}\frac{\partial \eta}{\partial x}\right\}$$

$$+ \overline{\overline{H}}\frac{1}{J}\left\{\frac{\partial \vec{a}}{\partial \xi}\frac{\partial \xi}{\partial y}+\frac{\partial \vec{a}}{\partial \eta}\frac{\partial \eta}{\partial y}\right\} + \frac{1}{\mathrm{Re}}\frac{1}{J}\left\{\frac{\partial \vec{c}}{\partial \xi}\frac{\partial \xi}{\partial y}+\frac{\partial \vec{c}}{\partial \eta}\frac{\partial \eta}{\partial y}\right\} = 0 \qquad (7)$$

Identities of the form,

$$\frac{\partial\left(\vec{b}\xi_x/J\right)}{\partial \xi} = \frac{\partial \vec{b}}{\partial \xi}\left(\frac{\xi_x}{J}\right) + \vec{b}\frac{\partial(\xi_x/J)}{\partial \xi} \qquad (8)$$

can be used to rewrite the governing equations as,

$$\frac{\partial(\vec{a}/J)}{\partial t} + \overline{\overline{G}}\frac{\partial}{\partial \xi}\left(\frac{\vec{a}\xi_x}{J}\right)+\overline{\overline{H}}\frac{\partial}{\partial \xi}\left(\frac{\vec{a}\xi_y}{J}\right)+\overline{\overline{G}}\frac{\partial}{\partial \eta}\left(\frac{\vec{a}\eta_x}{J}\right)+\overline{\overline{H}}\frac{\partial}{\partial \eta}\left(\frac{\vec{a}\eta_y}{J}\right)$$

$$+ \frac{1}{\mathrm{Re}}\left\{\frac{\partial}{\partial \xi}\left(\frac{\vec{b}\xi_x}{J}+\frac{\vec{c}\xi_y}{J}\right)+\frac{\partial}{\partial \eta}\left(\frac{\vec{b}\eta_x}{J}+\frac{\vec{c}\eta_y}{J}\right)\right\}$$

$$-\left\{\frac{\vec{c}}{\mathrm{Re}}+\overline{\overline{G}}\,\vec{a}\right\}\left\{\frac{\partial}{\partial \xi}\left(\frac{\xi_x}{J}\right)+\frac{\partial}{\partial \eta}\left(\frac{\eta_x}{J}\right)\right\} \qquad (9)$$

$$-\left\{\frac{\vec{b}}{\mathrm{Re}}+\overline{\overline{H}}\,\vec{a}\right\}\left\{\frac{\partial}{\partial \xi}\left(\frac{\xi_y}{J}\right)+\frac{\partial}{\partial \eta}\left(\frac{\eta_y}{J}\right)\right\} = 0$$

where J is not a function in time $J \neq f(t)$. The second last term vanishes since,

$$\left\{\left(\frac{\xi_x}{J}\right)_\xi+\left(\frac{\eta_x}{J}\right)_\eta\right\} = \left\{\left(y_\eta\right)_\xi+\left(-y_\xi\right)_\eta\right\} = \left\{\frac{\partial^2 y}{\partial \xi \partial \eta}-\frac{\partial^2 y}{\partial \eta \partial \xi}\right\} \qquad (10)$$

The last term also vanishes in a similar manner. The governing equations can now be expressed in general coordinates as,

$$\frac{\partial \hat{a}}{\partial t} + \overline{\overline{G}}\frac{\partial \hat{e}}{\partial \xi}+\overline{\overline{H}}\frac{\partial \hat{f}}{\partial \xi}+\overline{\overline{G}}\frac{\partial \hat{g}}{\partial \eta}+\overline{\overline{H}}\frac{\partial \hat{h}}{\partial \eta}+\frac{1}{\mathrm{Re}}\left\{\frac{\partial \hat{b}}{\partial \xi}+\frac{\partial \hat{c}}{\partial \eta}\right\} = 0 \qquad (11)$$

where the vectors in equation (11) are described as,

$$\hat{a} = \left\{\frac{\bar{a}}{J}\right\}, \quad \hat{e} = (\hat{a}\xi_x), \quad \hat{f} = (\hat{a}\xi_y), \quad \hat{g} = (\hat{a}\eta_x), \quad \hat{h} = (\hat{a}\eta_y),$$

and

$$\hat{b} = \left\{\frac{\bar{b}\xi_x}{J} + \frac{\bar{c}\xi_y}{J}\right\}, \quad \hat{c} = \left\{\frac{\bar{b}\eta_x}{J} + \frac{\bar{c}\eta_y}{J}\right\}$$

After multiplying through with the tensors $\overline{\overline{G}}$ and $\overline{\overline{H}}$, the components can be fully listed. The inviscid components are:

$$\overline{\overline{G}}\frac{\partial \hat{e}}{\partial \xi} = \begin{bmatrix} 2\bar{U}(u\xi_x/J)_\xi + \bar{V}(v\xi_x/J)_\xi + (P\xi_x/J)_\xi \\ \bar{U}(v\xi_x/J)_\xi \\ \beta^2(u\xi_x/J)_\xi \end{bmatrix} \tag{12a}$$

$$\overline{\overline{H}}\frac{\partial \hat{f}}{\partial \xi} = \begin{bmatrix} \bar{V}(u\xi_y/J)_\xi \\ \bar{U}(u\xi_y/J)_\xi + 2\bar{V}(v\xi_y/J)_\xi + (P\xi_y/J)_\xi \\ \beta^2(v\xi_y/J)_\xi \end{bmatrix} \tag{12b}$$

$$\overline{\overline{G}}\frac{\partial \hat{g}}{\partial \eta} = \begin{bmatrix} 2\bar{U}(u\eta_x/J)_\eta + \bar{V}(v\eta_x/J)_\eta + (P\eta_x/J)_\eta \\ \bar{U}(v\eta_x/J)_\eta \\ \beta^2(u\eta_x/J)_\eta \end{bmatrix} \tag{12c}$$

$$\overline{\overline{H}}\frac{\partial \hat{h}}{\partial \eta} = \begin{bmatrix} \bar{V}(u\eta_y/J)_\eta \\ \bar{U}(u\eta_y/J)_\eta + 2\bar{V}(v\eta_y/J)_\eta + (P\eta_y/J)_\eta \\ \beta^2(v\eta_y/J)_\eta \end{bmatrix} \tag{12d}$$

while the viscous components of equation (11) are fully listed as:

$$\frac{\partial \hat{b}}{\partial \xi} = \frac{\partial}{\partial \xi} \frac{1}{J\ \mathrm{Re}} \begin{bmatrix} \xi_x \dfrac{\partial u}{\partial x} + \xi_y \dfrac{\partial u}{\partial y} \\ \xi_x \dfrac{\partial v}{\partial x} + \xi_y \dfrac{\partial v}{\partial y} \\ 0 \end{bmatrix}$$

$$= \frac{1}{\mathrm{Re}} \frac{\partial}{\partial \xi} \frac{1}{J} \begin{bmatrix} \xi_x \left(\xi_x \dfrac{\partial u}{\partial \xi} + \eta_x \dfrac{\partial u}{\partial \eta} \right) + \xi_y \left(\xi_y \dfrac{\partial u}{\partial \xi} + \eta_y \dfrac{\partial u}{\partial \eta} \right) \\ \xi_x \left(\xi_x \dfrac{\partial v}{\partial \xi} + \eta_x \dfrac{\partial v}{\partial \eta} \right) + \xi_y \left(\xi_y \dfrac{\partial v}{\partial \xi} + \eta_y \dfrac{\partial v}{\partial \eta} \right) \\ 0 \end{bmatrix} \tag{12e}$$

$$\frac{\partial \hat{c}}{\partial \eta} = \frac{\partial}{\partial \eta} \frac{1}{J\ \mathrm{Re}} \begin{bmatrix} \eta_x \dfrac{\partial u}{\partial x} + \eta_y \dfrac{\partial u}{\partial y} \\ \eta_x \dfrac{\partial v}{\partial x} + \eta_y \dfrac{\partial v}{\partial y} \\ 0 \end{bmatrix}$$

$$= \frac{1}{\mathrm{Re}} \frac{\partial}{\partial \eta} \frac{1}{J} \begin{bmatrix} \eta_x \left(\xi_x \dfrac{\partial u}{\partial \xi} + \eta_x \dfrac{\partial u}{\partial \eta} \right) + \eta_y \left(\xi_y \dfrac{\partial u}{\partial \xi} + \eta_y \dfrac{\partial u}{\partial \eta} \right) \\ \eta_x \left(\xi_x \dfrac{\partial v}{\partial \xi} + \eta_x \dfrac{\partial v}{\partial \eta} \right) + \eta_y \left(\xi_y \dfrac{\partial v}{\partial \xi} + \eta_y \dfrac{\partial v}{\partial \eta} \right) \\ 0 \end{bmatrix} \tag{12f}$$

Thin-Layer Approximation

In flows which have a high Reynolds number, the computational effort to solve the governing set of equations may be reduced by only evaluating the viscous derivatives that are perpendicuar to the surface of the body. In these types of flows, the largest gradients occur in the direction normal to the surface so deleting the viscous derivatives parallel to the surface do not greatly affect the solution. This is referred to as the Thin-layer approximation. In non-parallel flows, however, the direction of large gradients may not be evident. The computational effort may still be reduced by deleting the cross derivatives. This is equivalent to using the Thin-layer approximation in each coordinate direction. Applying this strategy to the viscous derivatives gives:

$$\frac{\partial \hat{c}}{\partial \eta} = \frac{1}{\mathrm{Re}} \frac{\partial}{\partial \eta} \frac{1}{J} \begin{bmatrix} \left(\eta_x^2 + \eta_y^2\right) \dfrac{\partial u}{\partial \eta} \\ \left(\eta_x^2 + \eta_y^2\right) \dfrac{\partial v}{\partial \eta} \\ 0 \end{bmatrix} \tag{13a}$$

$$\frac{\partial \hat{b}}{\partial \xi} = \frac{1}{\mathrm{Re}} \frac{\partial}{\partial \xi} \frac{1}{J} \begin{bmatrix} \left(\xi_x^2 + \xi_y^2\right) \dfrac{\partial u}{\partial \xi} \\ \left(\xi_x^2 + \xi_y^2\right) \dfrac{\partial v}{\partial \xi} \\ 0 \end{bmatrix} \tag{13b}$$

Flux Linearization

The solution of the adjoint set of equations will be accomplished in an implicit manner to take advantage of larger time steps without encountering problems with stiffness in the equations. The implicit formulation will require that the fluxes be linearized. Linearization is possible if, for example, in the representative wave equation,

$$\frac{\partial \hat{a}}{\partial t}+\frac{\partial \hat{b}}{\partial x}=0 \tag{14}$$

the vector $\hat{b}$ is a homogeneous function of degree one in $\hat{a}$. The vector $\hat{b}$ may then be described as (Ref. 6),

$$f\left(\alpha \hat{b}\right)=\alpha f\left(\hat{b}\right) \tag{15}$$

for all $\hat{a}$. The diferential involving $\hat{b}$ in the representative wave equation may then be written as,

$$\frac{\partial \hat{b}}{\partial x}=\frac{\partial \hat{a}}{\partial x}\frac{\partial \hat{b}}{\partial \hat{a}}=[B]\frac{\partial \hat{a}}{\partial x} \tag{16}$$

where $[B]$ is held locally constant. Applying this to the adjoint set of equations (11) gives,

$$\frac{\partial \hat{a}}{\partial t}+\overline{\overline{G}}\,[\xi_x]\frac{\partial \hat{a}}{\partial \xi}+\overline{\overline{H}}\,[\xi_y]\frac{\partial \hat{a}}{\partial \xi}+\overline{\overline{G}}\,[\eta_x]\frac{\partial \hat{a}}{\partial \eta}+\overline{\overline{H}}\,[\eta_y]\frac{\partial \hat{a}}{\partial \eta}+\frac{1}{\mathrm{Re}}\left\{[B]\frac{\partial \hat{a}}{\partial \xi}+[C]\frac{\partial \hat{a}}{\partial \eta}\right\}=0 \tag{17a}$$

where,

$$[B]=\frac{\partial \hat{b}}{\partial \hat{a}}=\begin{bmatrix}\left(\xi_x^2+\xi_y^2\right)\frac{\partial}{\partial \xi} & 0 & 0\\ 0 & \left(\xi_x^2+\xi_y^2\right)\frac{\partial}{\partial \xi} & 0\\ 0 & 0 & 0\end{bmatrix} \tag{17b}$$

$$[C]=\frac{\partial \hat{c}}{\partial \hat{a}}=\begin{bmatrix}\left(\eta_x^2+\eta_y^2\right)\frac{\partial}{\partial \eta} & 0 & 0\\ 0 & \left(\eta_x^2+\eta_y^2\right)\frac{\partial}{\partial \eta} & 0\\ 0 & 0 & 0\end{bmatrix} \tag{17c}$$

Delta Form

The governing equations (11) must be cast in delta form to allow solution in an implicit manner. This form follows directly from writting the governing equations at the time step (n+1).

$$\frac{\partial \hat{a}^{(n+1)}}{\partial t} + \overline{\overline{G}}\frac{\partial \hat{e}^{(n+1)}}{\partial \xi} + \overline{\overline{H}}\frac{\partial \hat{f}^{(n+1)}}{\partial \xi} + \overline{\overline{G}}\frac{\partial \hat{g}^{(n+1)}}{\partial \eta} + \overline{\overline{H}}\frac{\partial \hat{h}^{(n+1)}}{\partial \eta} + \frac{1}{\mathrm{Re}}\left\{\frac{\partial \hat{b}}{\partial \xi} + \frac{\partial \hat{c}}{\partial \eta}\right\}^{(n+1)} = 0 \tag{18}$$

A first order estimate of the fluxes at time (n+1) can be made in the following manner:

$$\hat{b}^{(n+1)} = \hat{b}^{(n)} + \left[\frac{\partial \hat{b}}{\partial \hat{a}}\right]^{(n)}\left(\frac{\partial \hat{a}}{\partial t}\right)dt = \hat{b}^{(n)} + [B]^{(n)}(\delta \hat{a})^{(n+1)} \tag{19}$$

The governing equations may then be recast as,

$$\begin{aligned}
&\frac{(\delta \hat{a})^{(n+1)}}{\Delta t} + \overline{\overline{A}}\frac{\partial}{\partial \xi}\left\{\hat{e}^{(n)} + [\xi_x]^{(n)}(\delta \hat{a})^{(n+1)}\right\} + \overline{\overline{B}}\frac{\partial}{\partial \xi}\left\{\hat{f}^{(n)} + [\xi_y]^{(n)}(\delta \hat{a})^{(n+1)}\right\} \\
&+\overline{\overline{A}}\frac{\partial}{\partial \eta}\left\{\hat{g}^{(n)} + [\eta_x]^{(n)}(\delta \hat{a})^{(n+1)}\right\} + \overline{\overline{B}}\frac{\partial}{\partial \eta}\left\{\hat{h}^{(n)} + [\eta_y]^{(n)}(\delta \hat{a})^{(n+1)}\right\} \\
&+\frac{1}{\mathrm{Re}}\frac{\partial}{\partial \xi}\left\{\hat{b}^{(n)} + [C]^{(n)}(\delta \hat{a})^{(n+1)}\right\} + \frac{1}{\mathrm{Re}}\frac{\partial}{\partial \eta}\left\{\hat{c}^{(n)} + [D]^{(n)}(\delta \hat{a})^{(n+1)}\right\} = 0
\end{aligned} \tag{20}$$

Regrouping gives,

$$\begin{aligned}
&\left[I + \Delta t\left\{\overline{\overline{G}}\frac{\partial}{\partial \xi}[\xi_x]^{(n)} + \overline{\overline{H}}\frac{\partial}{\partial \xi}[\xi_y]^{(n)} + \overline{\overline{G}}\frac{\partial}{\partial \eta}[\eta_x]^{(n)} + \overline{\overline{H}}\frac{\partial}{\partial \eta}[\eta_y]^{(n)}\right.\right. \\
&\left.\left. + \frac{1}{\mathrm{Re}}\frac{\partial}{\partial \xi}[B]^{(n)} + \frac{1}{\mathrm{Re}}\frac{\partial}{\partial \eta}[C]^{(n)}\right\}\right](\delta \hat{a})^{(n+1)} = \\
&-\Delta t\left\{\overline{\overline{G}}\frac{\partial \hat{e}}{\partial \xi} + \overline{\overline{H}}\frac{\partial \hat{f}}{\partial \xi} + \overline{\overline{G}}\frac{\partial \hat{g}}{\partial \eta} + \overline{\overline{H}}\frac{\partial \hat{h}}{\partial \eta} + \frac{1}{\mathrm{Re}}\left(\frac{\partial \hat{b}}{\partial \xi} + \frac{\partial \hat{c}}{\partial \eta}\right)\right\}^{(n)}
\end{aligned} \tag{21}$$

Approximate Factorization

Directly inverting the left-hand-side of eqn. (21) is prohibitively expensive. If, instead, the LHS is factored in the following form:

$$\left[I+\Delta t\left\{\overline{\overline{G}}\frac{\partial}{\partial\xi}[\xi_x]^{(n)}+\overline{\overline{H}}\frac{\partial}{\partial\xi}[\xi_y]^{(n)}+\frac{1}{\mathrm{Re}}\frac{\partial}{\partial\xi}[B]^{(n)}\right\}\right]$$

$$\left[I+\Delta t\left\{\overline{\overline{G}}\frac{\partial}{\partial\eta}[\eta_x]^{(n)}+\overline{\overline{H}}\frac{\partial}{\partial\eta}[\eta_y]^{(n)}+\frac{1}{\mathrm{Re}}\frac{\partial}{\partial\eta}[C]^{(n)}\right\}\right](\delta\hat{a})^{(n+1)}=RHS \tag{22}$$

two tridiagonal block matrix systems are created which are easier to invert. Many schemes are available which are optimized for the inversion of block tri-diagonal systems. Multiplying out the LHS of eqn. (29) gives,

$$\left[I+\Delta t\left\{\overline{\overline{G}}\frac{\partial}{\partial\xi}[\xi_x]^{(n)}+\overline{\overline{H}}\frac{\partial}{\partial\xi}[\xi_y]^{(n)}+\frac{1}{\mathrm{Re}}\frac{\partial}{\partial\xi}[B]^{(n)}\right\}\right.$$

$$\left.+\Delta t\left\{\overline{\overline{G}}\frac{\partial}{\partial\eta}[\eta_x]^{(n)}+\overline{\overline{H}}\frac{\partial}{\partial\eta}[\eta_y]^{(n)}+\frac{1}{\mathrm{Re}}\frac{\partial}{\partial\eta}[C]^{(n)}\right\}\right. \tag{23}$$

$$\Delta t^2\left\{\overline{\overline{G}}\frac{\partial}{\partial\xi}[\xi_x]+\overline{\overline{H}}\frac{\partial}{\partial\xi}[\xi_y]+\frac{1}{\mathrm{Re}}\frac{\partial}{\partial\xi}[B]\right\}\left\{\overline{\overline{G}}\frac{\partial}{\partial\eta}[\eta_x]+\overline{\overline{H}}\frac{\partial}{\partial\eta}[\eta_y]+\frac{1}{\mathrm{Re}}\frac{\partial}{\partial\eta}[C]\right\}^{(n)}$$

$$=RHS$$

The last term is of order (Δt^2). Thus, the accuracy of the scheme is not impaired.

Artificial Dissipation

Central differencing is utilized for the convective terms. Therefore, artificial dissipation must be supplied to improve the stability characteristics of the relaxation scheme. Fourth order smoothing terms will be added to the RHS, while second order smoothing will be added to the LHS. The explicit smoothing term will have the form:

$$+\Delta t \in_e J^{-1}\left(\delta_\xi^4 + \delta_\eta^4\right) J[\hat{a}] \tag{24}$$

where δ_ξ^4 and δ_η^4 represent fourth order diferencing terms in the ξ and η directions, respectively. This method of smoothing can not be used on the implicit side because it woud create pentadiagonal block matrices. Solving such a system requires greater computational effort, therefore, the implicit smoothing terms will be of second order:

$$+\Delta t \in_i J^{-1}\left(\delta_\xi^2\right) J \qquad \text{and} \qquad +\Delta t \in_i J^{-1}\left(\delta_\eta^2\right) J \tag{25}$$

Here δ^2 represents a second order diference operator.

Computational Concerns

Examination of the governing equation (11) shows that the diffusive terms have a positive sign. If this equation were to be marched in time it would be unconditionally unstable since the contribution from this term would grow without bound. The convective terms are neutrally stable (in the sense that they have no bias with respect to time). Therefore, to reach a converged state the governing set of equations must be marched backward in time (negative time step). This is consistent with the idea behind the adjoint equations since we are tracing the result back to the source. For this reason, the smoothing terms (eqns. 24 and 25) are written with a positive sign.

Summary

The equations adjoint to the incompressible Navier-Stokes characterize the linear response of the flow field to a small disturbance. The adjoint field obtained from their solution maps the effectiveness of a control method to alter the flow. This work has, for the first time, formulated these equations in a manner that allows their solution with computational fluid dynamics techniques. It has addressed computational issues of discretization, pseudo-compressibility, flux linearization, implicit formulation, approximate factorization and artificial dissipation. A method of solution has been postulated that will overcome the instability inherent in the governing equations.

References

1. Abergel, F. and Temam, R. 1990, "On some control problems in fluid mechanics." Theoret. Comput. Fluid Dynamics, **1**, 303.

2. Jameson, A., "Aerodynamic Design Via Control Theory", 12th IMACS World Congress on Scientific Computation, July 1988.

3. Lighthill, M. J., "A New Method of Two Dimensional Aerodynamic Design", ARC, Rand M 2112, 1945

4. Hill, D. C., "A Theoretical Approach for Analyzing the Restabilization of Wakes," AIAA Paper No. 92-0067, 30th Aerospace Sciences Meeting, January 1992.

5. Hirch, C., *Numerical Computation of Internal and External Flows* , Vol. 2, Wiley, , New York, 1992, 656-661.

6. Steger, J. L. and Warming, R.F., "Flux Vector Splitting of the Inviscid Gasdynamic Equations with Applications to Finite-Difference Methods,"*J. Comp. Phys.* **40** (1981), 263--293.